

Homobinuclear cyanide-bridged linkage isomers containing the redox-active unit $[(\mu\text{-XY})\text{Ru}(\text{CO})_2\text{L}(\text{o-O}_2\text{C}_6\text{Cl}_4)]$ (XY = CN or NC)

Christopher J. Adams, Jonathan P. H. Charmant, Neil G. Connelly,* Martin Gill, Anob Kantacha, Sriwipa Onganusorn and A. Guy Orpen

Received 15th January 2007, Accepted 27th February 2007

First published as an Advance Article on the web 27th March 2007

DOI: 10.1039/b700648a

The salts $[\text{NEt}_4][\text{Ru}(\text{CN})(\text{CO})_2\text{L}(\text{o-O}_2\text{C}_6\text{Cl}_4)]$ {L = PPh₃ or P(OPh)₃}, which undergo one-electron oxidation at the catechol ligand to give neutral semiquinone complexes $[\text{Ru}(\text{CN})(\text{CO})_2\text{L}(\text{o-O}_2\text{C}_6\text{Cl}_4)]$, react with the dimers $\{[\text{Ru}(\text{CO})_2\text{L}(\mu\text{-o-O}_2\text{C}_6\text{Cl}_4)]_2\}$ {L = PPh₃ or P(OPh)₃} to give $[\text{NEt}_4][(\text{o-O}_2\text{C}_6\text{Cl}_4)\text{L}(\text{OC})_2\text{Ru}(\mu\text{-CN})\text{Ru}(\text{CO})_2\text{L}'(\text{o-O}_2\text{C}_6\text{Cl}_4)]$ {L or L' = PPh₃ or P(OPh)₃}. The cyanide-bridged binuclear anions are, in turn, reversibly oxidised to isolable neutral and cationic complexes $[(\text{o-O}_2\text{C}_6\text{Cl}_4)\text{L}(\text{OC})_2\text{Ru}(\mu\text{-CN})\text{Ru}(\text{CO})_2\text{L}'(\text{o-O}_2\text{C}_6\text{Cl}_4)]$ and $[(\text{o-O}_2\text{C}_6\text{Cl}_4)\text{L}(\text{OC})_2\text{Ru}(\mu\text{-CN})\text{Ru}(\text{CO})_2\text{L}'(\text{o-O}_2\text{C}_6\text{Cl}_4)]^+$ which contain one and two semiquinone ligands respectively. Structural studies on the redox pair $[(\text{o-O}_2\text{C}_6\text{Cl}_4)(\text{Ph}_3\text{P})(\text{OC})_2\text{Ru}(\mu\text{-CN})\text{Ru}(\text{CO})_2(\text{PPh}_3)(\text{o-O}_2\text{C}_6\text{Cl}_4)]^-$ and $[(\text{o-O}_2\text{C}_6\text{Cl}_4)(\text{Ph}_3\text{P})(\text{OC})_2\text{Ru}(\mu\text{-CN})\text{Ru}(\text{CO})_2(\text{PPh}_3)(\text{o-O}_2\text{C}_6\text{Cl}_4)]$ confirm that the C-bound $\text{Ru}(\text{CO})_2(\text{o-O}_2\text{C}_6\text{Cl}_4)$ fragment is oxidised first. Uniquely, $[(\text{o-O}_2\text{C}_6\text{Cl}_4)(\text{PhO})_3\text{P}](\text{OC})_2\text{Ru}(\mu\text{-CN})\text{Ru}(\text{CO})_2(\text{PPh}_3)(\text{o-O}_2\text{C}_6\text{Cl}_4)]^-$ is oxidised first at the N-bound fragment, indicating that it is possible to control the site of electron transfer by tuning the co-ligands. Crystallisation of $[(\text{o-O}_2\text{C}_6\text{Cl}_4)(\text{Ph}_3\text{P})(\text{OC})_2\text{Ru}(\mu\text{-CN})\text{Ru}(\text{CO})_2\{P(\text{OPh})_3\}(\text{o-O}_2\text{C}_6\text{Cl}_4)]$ resulted in the formation of an isomer in which the P(OPh)₃ ligand is *cis* to the cyanide bridge, contrasting with the *trans* arrangement of the X–Ru–L fragment in all other complexes of the type $\text{RuX}(\text{CO})_2\text{L}(\text{o-O}_2\text{C}_6\text{Cl}_4)$.

Introduction

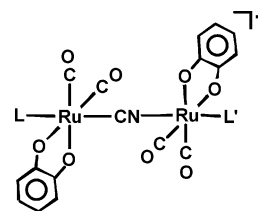
Our extensive studies of cyanide-bridged complexes containing low valent metal-based redox centres¹ have most recently involved the synthesis of paramagnetic species such as $[(\text{H}_3\text{N})_3\text{Ru}^{\text{III}}(\mu\text{-NC})\text{-Mn}^{\text{I}}(\text{CO})(\text{dppm})_2\text{-trans}][\text{PF}_6]_3$ in which intramolecular metal–metal charge transfer leads to strong solvatochromism.² In this paper we describe new monomeric cyanide complexes, $[\text{Ru}(\text{CN})(\text{CO})_2\text{L}(\text{o-O}_2\text{C}_6\text{Cl}_4)]^-$, which act as N-donor ligands in the formation of cyanide-bridged species with two ligand-based redox centres, namely $[(\text{o-O}_2\text{C}_6\text{Cl}_4)\text{L}(\text{OC})_2\text{Ru}(\mu\text{-XY})\text{Ru}(\text{CO})_2\text{-L}'(\text{o-O}_2\text{C}_6\text{Cl}_4)]^-$ {XY = CN or NC, L or L' = PPh₃ or P(OPh)₃} (Scheme 1). The two Ru(II)-bound catechol ligands are sequentially oxidised to semiquinones with the linkage isomers $[(\text{o-O}_2\text{C}_6\text{Cl}_4)(\text{Ph}_3\text{P})(\text{OC})_2\text{Ru}(\mu\text{-CN})\text{Ru}(\text{CO})_2\{P(\text{OPh})_3\}(\text{o-O}_2\text{C}_6\text{Cl}_4)]^-$ and $[(\text{o-O}_2\text{C}_6\text{Cl}_4)(\text{Ph}_3\text{P})(\text{OC})_2\text{Ru}(\mu\text{-NC})\text{Ru}(\text{CO})_2\{P(\text{OPh})_3\}(\text{o-O}_2\text{C}_6\text{Cl}_4)]^-$ first oxidised at the C-bound and N-bound $\text{Ru}(\text{CO})_2\text{-}(\text{PPh}_3)(\text{o-O}_2\text{C}_6\text{Cl}_4)$ group respectively.

Results and discussion

The synthesis and characterisation of $\{[\text{Ru}(\text{CO})_2\text{L}(\mu\text{-o-O}_2\text{C}_6\text{Cl}_4)]_2\}$

In order to synthesise the new anionic cyanide complexes $[\text{Ru}(\text{CN})(\text{CO})_2\text{L}(\text{o-O}_2\text{C}_6\text{Cl}_4)]^-$ described below, the dimeric precursors $\{[\text{Ru}(\text{CO})_2\text{L}(\mu\text{-o-O}_2\text{C}_6\text{Cl}_4)]_2\}$ {L = PPh₃ or P(OPh)₃} were

School of Chemistry, University of Bristol, Bristol, UK BS8 1TS. E-mail: neil.connelly@bristol.ac.uk; Fax: +44 (0)117 929 0509; Tel: +44 (0)117 928 8162



Complex	L	L'
8⁻	PPh ₃	PPh ₃
9⁻	PPh ₃	P(OPh) ₃
10⁻	P(OPh) ₃	P(OPh) ₃
11⁻	P(OPh) ₃	PPh ₃

Scheme 1 Complexes $[(\text{o-O}_2\text{C}_6\text{Cl}_4)\text{L}(\text{OC})_2\text{Ru}(\mu\text{-CN})\text{Ru}(\text{CO})_2\text{L}'(\text{o-O}_2\text{C}_6\text{Cl}_4)]^-$.

first prepared, the former by the published method involving the reaction of tetrachlorobenzene-*o*-quinone (*o*-chloranil) with $[\text{Ru}(\text{CO})_2(\text{PPh}_3)(\eta\text{-C}_4\text{H}_4\text{Me}_2)]^3$ and the latter by a modification thereof.

Thus, heating a mixture of $[\text{Ru}_3(\text{CO})_{12}]$ and 2,3-dimethylbuta-1,3-diene in *n*-heptane under reflux for 23 h, adding P(OPh)₃, heating the mixture for a further 6 d and then purifying the product by column chromatography gave $[\text{Ru}(\text{CO})_2\{P(\text{OPh})_3\}(\eta\text{-C}_4\text{H}_4\text{Me}_2)]$ as a white solid in moderate yield. Subsequent reaction of $[\text{Ru}(\text{CO})_2\{P(\text{OPh})_3\}(\eta\text{-C}_4\text{H}_4\text{Me}_2)]$ with *o*-chloranil at room temperature in CH₂Cl₂ rapidly gave an orange solution from which $\{[\text{Ru}(\text{CO})_2\{P(\text{OPh})_3\}(\mu\text{-o-O}_2\text{C}_6\text{Cl}_4)]_2\}$ was isolated in high yield

Table 1 Analytical, IR spectroscopic and cyclic voltammetric data for ruthenium dicarbonyl complexes

Complex	Colour	Yield (%)	Analysis (%) ^a		IR/cm ⁻¹ ^b		<i>E</i> _o / V
			C	H	N	<i>v</i> (CN)	
[Ru(CO) ₂ {P(OPh) ₃ }(η-C ₆ H ₄ Me)]	White	32	56.9 (56.8)	4.7 (4.6)	—	2012, 1951	—
[{Ru(CO) ₂ (PPh ₃) ₂ (μ-O ₂ C ₆ Cl ₄) ₂ }] ^d	—	—	—	—	—	2065sh, 2054, 2002, 1984m	—
[{Ru(CO) ₂ (P(OPh) ₃) ₂ (μ-O ₂ C ₆ Cl ₄) ₂ }]	Orange	79	43.9 (43.8)	2.0 (2.1)	—	2081, 2075, 2025, 2014	—
[Ru(CN)(CO) ₂ (P(OPh) ₃)(μ-O ₂ C ₆ Cl ₄)] ^e	Yellow	68	51.3 (51.1)	4.4 (4.3)	3.6 (3.4)	2127w	0.44, 1.52(1) ^f
[Ru(CN)(CO) ₂ {P(OPh) ₃ }(μ-O ₂ C ₆ Cl ₄)] ^e 2⁻	Yellow	52	48.2 (48.4)	4.1 (4.1)	3.2 (3.2)	2065, 2003	0.51, 1.67(1) ^f
[Ru(CO) ₂ (NCMe)(PPh ₃)(μ-O ₂ C ₆ Cl ₄)]	Yellow	54	47.3 (47.6)	2.6 (2.6)	1.9 (2.0)	2132w	0.79, 1.65(1)
[Ru(CO) ₂ {P(OPh) ₃ }(μ-O ₂ C ₆ Cl ₄)]	Yellow	46	51.6 (51.6)	3.0 (2.9)	—	2056, 1992	0.79 ^g
[Ru(CO) ₂ (PPh ₃) ₂ {(μ-O ₂ C ₆ Cl ₄)}] ^d	—	—	—	—	—	2074, 2018	0.68, 1.75(1) ^h
[Ru(CO) ₂ (PPh ₃) ₂ {(μ-O ₂ C ₆ Cl ₄)}] ^d	—	—	—	—	—	2060, 2001	0.59, 1.62 ^h
[Ru(CO) ₂ (PPh ₃) ₂ {(μ-O ₂ C ₆ Cl ₄)}] ^d	—	—	—	—	—	2045, 1983	—

^a Calculated values in parentheses. ^b Strong absorptions in CH₂Cl₂; unless otherwise stated; w = weak, m = medium, sh = shoulder. ^c At a Pt electrode in CH₂Cl₂, with potentials relative to the saturated calomel electrode, calibrated vs. the [Fe(η-C₅H₅)₂]/[Fe(η-C₅H₅)₂]⁺/[Fe(η-C₅H₅)₂]⁺ couple (at 0.47 V) unless otherwise stated. For an irreversible (I) process, the oxidation peak potential, (*E*_p)_{ox}, is given at a scan rate of 200 mV s⁻¹. ^d Data from ref. 3. ^e [NEt₄]⁺ salt. ^f Calibrated vs. the [Fe(η-C₅H₅)₂]/[Fe(η-C₅H₅)₂]⁺ couple (at 0.74 V). ^g Second oxidation not observed. ^h Data from ref. 3, corrected to the same internal potential standard used herein.

as an orange solid, characterised by elemental analysis and IR spectroscopy (Table 1).

The complex [{Ru(CO)₂{P(OPh)₃}(μ-*o*-O₂C₆Cl₄)₂}] shows four IR carbonyl bands, consistent with the dimeric structure proposed earlier³ for [{Ru(CO)₂(PPh₃)(μ-*o*-O₂C₆Cl₄)₂}], in which the *o*-O₂C₆Cl₄ ligand acts as a bridging *O*-donor, and now confirmed by the X-ray structure shown in Fig. 1 (with selected bond lengths and angles given in Table 2).

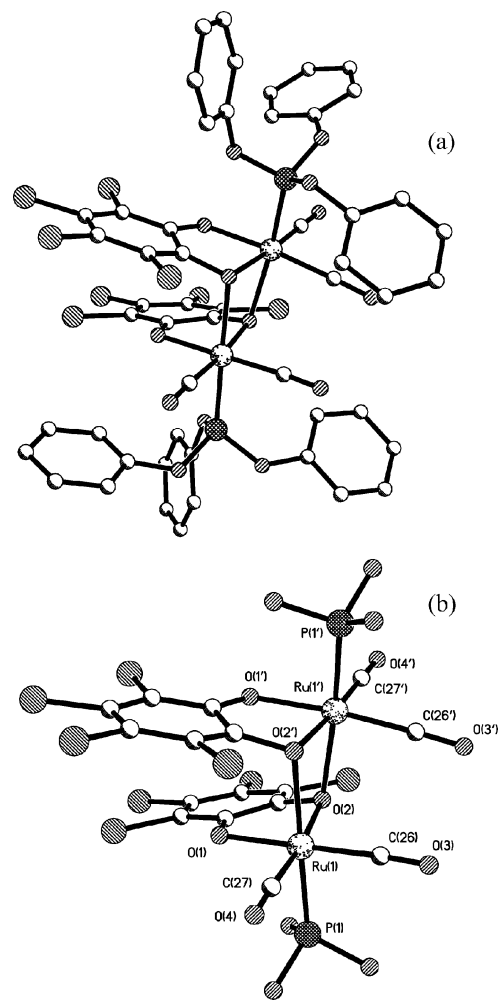


Fig. 1 The molecular structure of [{Ru(CO)₂{P(OPh)₃}(μ-*o*-O₂C₆Cl₄)₂}] (a), with hydrogen and chlorine atoms omitted for clarity. In (b) the core of the structure has been expanded, and the phenyl rings of the P(OPh)₃ ligands omitted, to show more clearly the bridging of the catecholate ligands and the atom labeling.

The dimer is composed of two edge-sharing six-coordinate ruthenium centres. Each ruthenium atom has an equatorial coordination set comprised of the two carbonyl groups and the bidentate O₂C₆Cl₄ ligand, with the triphenylphosphite ligand occupying an axial position. The dimer is then formed by bringing two of these subunits together such that the second axial site at each ruthenium is filled by one of the oxygen atoms of the O₂C₆Cl₄ ligand that chelates the other metal atom. The resulting Ru₂(μ-O)₂ core is asymmetric, with the axial Ru–O bonds longer than the equatorial {e.g. Ru(1)–O(2) = 2.110(1), Ru(1')–O(2) = 2.218(1) Å}, and with a fold angle of 15.7°. The Ru–O distances within

Table 2 Selected bond lengths (Å) and angles (°) for $[\{\text{Ru}(\text{CO})_2\text{P}(\text{O}(\text{Ph})_3)\}_2(\mu\text{-}o\text{-O}_2\text{C}_6\text{Cl}_4)_2]$

Ru(1)–P(1)	2.246(1)	Ru(1')–P(1')	2.248(1)
Ru(1)–O(1)	2.050(2)	Ru(1')–O(1')	2.047(2)
Ru(1)–O(2)	2.110(1)	Ru(1')–O(2')	2.103(1)
Ru(1)–O(2')	2.221(1)	Ru(1')–O(2)	2.218(1)
Ru(1)–C(26)	1.898(2)	Ru(1')–C(26')	1.910(2)
Ru(1)–C(27)	1.893(2)	Ru(1')–C(27')	1.884(2)
C(26)–O(3)	1.135(2)	C(26')–O(3')	1.136(2)
C(27)–O(4)	1.133(2)	C(27')–O(4')	1.133(3)
C(19)–O(1)	1.322(2)	C(19')–O(1')	1.330(2)
C(24)–O(2)	1.366(2)	C(24')–O(2')	1.373(2)
C(19)–C(20)	1.399(3)	C(19')–C(20')	1.397(3)
C(20)–C(21)	1.395(3)	C(20')–C(21')	1.401(3)
C(21)–C(22)	1.393(3)	C(21')–C(22')	1.387(3)
C(22)–C(23)	1.394(3)	C(22')–C(23')	1.403(3)
C(23)–C(24)	1.385(3)	C(23')–C(24')	1.383(3)
C(24)–C(19)	1.407(3)	C(24')–C(19')	1.404(3)
O(2')–Ru(1)–P(1)	174.44(4)	O(2)–Ru(1')–P(1')	168.31(4)
O(2)–Ru(1)–P(1)	95.18(4)	O(2')–Ru(1')–P(1')	88.74(4)
O(1)–Ru(1)–O(2)	79.56(6)	O(1')–Ru(1')–O(2')	80.41(6)
O(1)–Ru(1)–O(2')	88.22(6)	O(1')–Ru(1')–O(2)	87.50(6)
Ru(1)–O(2)–Ru(1')	99.18(6)	Ru(1)–O(2')–Ru(1')	99.31(6)
O(3)–C(26)–Ru(1)	176.02(18)	O(3')–C(26')–Ru(1')	172.11(18)
O(4)–C(27)–Ru(1)	177.54(18)	O(4')–C(27')–Ru(1')	178.4(2)

each ruthenium–catecholate ring also reflect the fact that one of the oxygen atoms is involved in an extra interaction {e.g. Ru(1)–O(1) = 2.050(2), Ru(1)–O(2) = 2.110(1) Å}.

The bridging behaviour of one catecholate oxygen atom also leads to a longer C–O distance within the chelate ring {e.g. C(19)–O(1) = 1.322(2) vs. C(24)–O(2) = 1.366(2) Å}. However, these C–O distances (and the C–C distances in the C₆ rings of the *o*-O₂C₆Cl₄ ligands) are similar to those in $[\{\text{MoO}(\text{o}-\text{O}_2\text{C}_6\text{H}_2\text{Bu}^t)_2\}_2]$,⁴ $[\{\text{M}(\text{py})_2(\text{o}-\text{O}_2\text{C}_6\text{H}_2\text{Bu}^t)_2\}_2]$,⁵ $[(\text{o}-\text{O}_2\text{C}_6\text{Cl}_4)(\text{Ph}_3\text{P})(\text{OC})_2\text{Ru}(\mu\text{-NC})\text{Mn}(\text{CO})_2(\text{PEt}_3)(\text{dppe})\text{-}cis]$,⁶ $[(\text{o}-\text{O}_2\text{C}_6\text{Cl}_4)(\text{Ph}_3\text{P})(\text{OC})_2\text{Ru}(\mu\text{-NC})\text{Re}(\text{CO})_3(\text{o}-phen)]$ ⁷ and $[\text{Pd}(\text{PPh}_3)_2(\text{o}-\text{O}_2\text{C}_6\text{Cl}_4)]$ ⁸ and are consistent with the *o*-O₂C₆Cl₄ ligand acting as a dianionic catecholate.

The bridging arrangement, and asymmetric catecholate bonding, in $[\{\text{Ru}(\text{CO})_2\{\text{P}(\text{O}(\text{Ph})_3)\}_2(\mu\text{-}o\text{-O}_2\text{C}_6\text{Cl}_4)_2]$ is also found in $[\{\text{MoO}(\text{o}-\text{O}_2\text{C}_6\text{H}_2\text{Bu}^t)_2\}_2]$ ⁴ and $[\{\text{M}(\text{py})_3(\text{o}-\text{O}_2\text{C}_6\text{H}_2\text{Bu}^t)_2\}_2]$ (M = Mn or Fe)⁵ but with one significant difference. Thus, in these cases the two catecholate rings are coplanar, *i.e.* mutually *trans* with respect to the M₂(μ-O)₂ core whereas those in $[\{\text{Ru}(\text{CO})_2\{\text{P}(\text{O}(\text{Ph})_3)\}_2(\mu\text{-}o\text{-O}_2\text{C}_6\text{Cl}_4)_2]$ are mutually *cis*.

The synthesis and characterisation of $[\text{NET}_4][\text{Ru}(\text{CN})(\text{CO})_2\text{L}(\text{o}-\text{O}_2\text{C}_6\text{Cl}_4)]$ {L = PPh₃ or P(OPh)₃}

The complexes $[\text{NET}_4][\text{Ru}(\text{CN})(\text{CO})_2\text{L}(\text{o}-\text{O}_2\text{C}_6\text{Cl}_4)]$ {L = PPh₃, $[\text{NET}_4]^+ \mathbf{1}^-$ or P(OPh)₃, $[\text{NET}_4]^+ \mathbf{2}^-$ } were prepared by adding two equivalents of $[\text{NET}_4]\text{CN}$ to $[\{\text{Ru}(\text{CO})_2\text{L}(\mu\text{-}o\text{-O}_2\text{C}_6\text{Cl}_4)_2\}]$ {L = PPh₃ or P(OPh)₃} in CH₂Cl₂ and then adding *n*-hexane to precipitate the yellow solids. The salts, soluble in solvents such as MeCN, thf and CH₂Cl₂ but not in less polar solvents such as toluene, *n*-hexane and diethyl ether, were characterised by elemental analysis and IR (Table 1) and NMR spectroscopy.

The IR spectra of $\mathbf{1}^-$ and $\mathbf{2}^-$ show one weak ν(CN) band, at *ca.* 2130 cm⁻¹, and two ν(CO) bands, at 2047 and 1983, and at 2065 and 2003 cm⁻¹, respectively. The ¹H NMR spectra are unremarkable, showing the expected signals for the $[\text{NET}_4]^+$ counterion and the phenyl protons of the *P*-donor ligands. However, the ³¹P NMR

spectra, showing singlets at δ 19.7 and 113.5 for the PPh₃ and P(OPh)₃ ligands of $\mathbf{1}^-$ and $\mathbf{2}^-$ respectively, are useful in aiding the assignment of the spectra of the binuclear species described below.

The X-ray structure of the anion $[\text{NET}_4]^+ \mathbf{1}^-$ is shown in Fig. 2 with selected bond lengths and angles in Table 3. (There are two essentially identical anions in the asymmetric unit.) The ruthenium atom is bonded to a cyanide ligand *trans* to PPh₃, two *cis* carbonyls and an *o*-O₂C₆Cl₄ chelate, in a slightly distorted octahedral geometry {e.g. the angles O(1)–Ru(1)–O(2) and C(26)–Ru(1)–O(1) are 80.96(8) and 173.60(12)° respectively}. The C–O bond distances in the Ru–chelate ring, averaging 1.32 Å, are again consistent with the *o*-O₂C₆Cl₄ ligand acting as a catecholate (as are the C–C distances within the C₆ ring). Similar structures have been determined for $[\text{Ru}(\text{CO})_2(\text{PPh}_3)_2(\text{o}-\text{O}_2\text{C}_6\text{Cl}_4)]$ ⁹ and $[\text{Ru}(\text{CO})_2(\text{PPh}_3)_2\text{L}]$ (H₂L = 7,8-dihydroxy-6-methylcoumarin).¹⁰

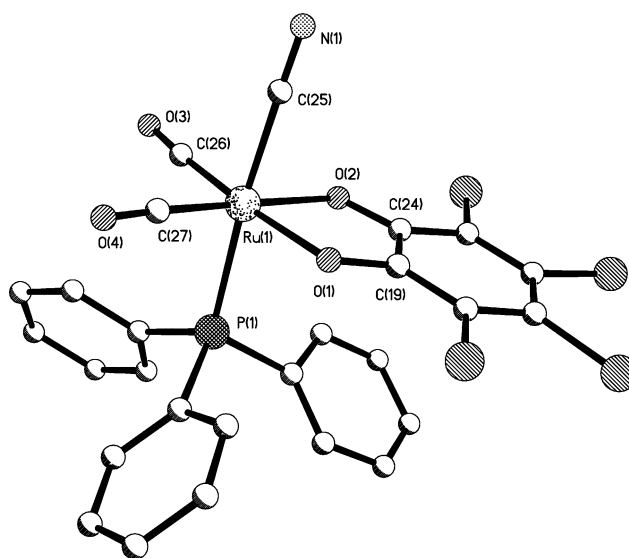


Fig. 2 The structure of the anion $[\text{Ru}(\text{CN})(\text{CO})_2(\text{PPh}_3)(\text{o}-\text{O}_2\text{C}_6\text{Cl}_4)]^- \mathbf{1}^-$. Hydrogen atoms have been omitted for clarity. The six-membered ring of the catecholate ligand ring is numbered from C(19) to C(24).

Each of the CVs of $[\text{NET}_4]^+ \mathbf{1}^-$ and $[\text{NET}_4]^+ \mathbf{2}^-$, at a Pt disc electrode in CH₂Cl₂, shows two oxidation waves, at 0.44 and 1.52 V and at 0.51 and 1.67 V, respectively (Table 1). In each case, the first wave is fully reversible, corresponding to the formation of the neutral complex $[\text{Ru}(\text{CN})(\text{CO})_2\text{L}(\text{o}-\text{O}_2\text{C}_6\text{Cl}_4)]$ {L = PPh₃, $\mathbf{1}$ or P(OPh)₃, $\mathbf{2}$ }; the second wave is irreversible (the peak potential is given at a scan rate of 200 mV s⁻¹) as a result of the instability of the monocation $[\text{Ru}(\text{CN})(\text{CO})_2\text{L}(\text{o}-\text{O}_2\text{C}_6\text{Cl}_4)]^+$ {L = PPh₃, $\mathbf{1}^+$ or P(OPh)₃, $\mathbf{2}^+$ }. The potential for the first oxidation of $\mathbf{1}^-$ is similar to those of the analogous halide anions $[\text{RuX}(\text{CO})_2(\text{PPh}_3)(\text{o}-\text{O}_2\text{C}_6\text{Cl}_4)]^-$ (X = Cl, 0.43 V; X = Br, 0.42 V; X = I, 0.38 V) but somewhat more negative (by 100–200 mV) than those of the neutral complexes $[\text{Ru}(\text{CO})_2(\text{PPh}_3)_2\text{L}(\text{o}-\text{O}_2\text{C}_6\text{Cl}_4)]$ {L = PPh₃, 0.59 V; L = P(OPh)₃, 0.68 V}.³

Like the complexes $[\text{RuX}(\text{CO})_2(\text{PPh}_3)(\text{o}-\text{O}_2\text{C}_6\text{Cl}_4)]^-$ (X = Cl, Br or I) and $[\text{Ru}(\text{CO})_2(\text{PPh}_3)_2\text{L}(\text{o}-\text{O}_2\text{C}_6\text{Cl}_4)]$ {L = PPh₃ or P(OPh)₃}, the cyanide derivatives $[\text{NET}_4]^+ \mathbf{1}^-$ and $[\text{NET}_4]^+ \mathbf{2}^-$ in CH₂Cl₂ react with a one-electron oxidant, $[\text{Fe}(\eta\text{-C}_5\text{H}_4\text{COMe})(\eta\text{-C}_5\text{H}_5)][\text{BF}_4]$ in these cases, to give deep purple solutions of the neutral

Table 3 Selected bond lengths (Å) and angles (°) for [Ru(CN)(CO)₂-(PPh₃)(*o*-O₂C₆Cl₄)]⁻ **1**^a

Ru(1)–O(2)	2.077(2)	C(26)–Ru(1)–C(27)	92.69(15)
Ru(1')–O(2')	2.080(2)	C(26')–Ru(1')–C(27')	91.70(16)
Ru(1)–O(1)	2.088(2)	C(25)–Ru(1)–P(1)	175.58(10)
Ru(1')–O(1')	2.091(2)	C(25')–Ru(1')–P(1')	176.66(11)
Ru(1)–P(1)	2.431(1)	O(1)–Ru(1)–O(2)	80.96(8)
Ru(1')–P(1')	2.417(1)	O(1')–Ru(1')–O(2')	80.24(8)
Ru(1)–C(25)	2.065(4)	C(27)–Ru(1)–O(2)	174.18(13)
Ru(1')–C(25')	2.068(4)	C(27')–Ru(1')–O(2')	175.65(13)
Ru(1)–C(27)	1.855(4)	C(26)–Ru(1)–O(1)	173.60(12)
Ru(1')–C(27')	1.870(4)	C(26')–Ru(1')–O(1')	172.19(12)
Ru(1)–C(26)	1.874(4)	C(25)–Ru(1)–C(27)	92.74(14)
Ru(1')–C(26')	1.860(4)	C(25')–Ru(1')–C(27')	90.00(14)
C(25)–N(1)	1.151(4)	C(25)–Ru(1)–C(26)	89.39(14)
C(25')–N(1')	1.154(4)	C(25')–Ru(1')–C(26')	90.02(15)
C(19)–O(1)	1.330(4)	C(27)–Ru(1)–P(1)	90.06(11)
C(19')–O(1')	1.336(4)	C(27')–Ru(1')–P(1')	89.48(10)
C(24)–O(2)	1.314(4)	C(26)–Ru(1)–P(1)	93.90(10)
C(24')–O(2')	1.318(4)	C(26')–Ru(1')–P(1')	93.30(11)
C(19)–C(20)	1.388(4)	O(1)–Ru(1)–C(27)	93.60(13)
C(19')–C(20')	1.383(4)	O(1')–Ru(1')–C(27')	96.11(12)
C(20)–C(21)	1.409(4)	O(2)–Ru(1)–C(26)	92.71(12)
C(20')–C(21')	1.410(4)	O(2')–Ru(1')–C(26')	91.95(13)
C(21)–C(22)	1.384(5)		
C(21')–C(22')	1.386(5)		
C(22)–C(23)	1.393(4)		
C(22')–C(23')	1.395(4)		
C(23)–C(24)	1.392(4)		
C(23')–C(24')	1.391(4)		
C(24)–C(19)	1.434(4)		
C(24')–C(19')	1.422(4)		

^a There are two independent molecules in the asymmetric unit. Equivalent atoms for the second are distinguished from the first by primes.

compounds [Ru(CN)(CO)₂L(*o*-O₂C₆Cl₄)] {L = PPh₃ **1** or P(OPh)₃ **2**}. Although these species could not be isolated (unlike their halide analogues³), they were characterised in solution as semiquinone derivatives of ruthenium(II) by IR spectroscopy. Thus, weak ν(CN) bands (at 2138 and 2142 cm⁻¹) are accompanied by strong ν(CO) bands, at 2077 and 2023 cm⁻¹ and at 2093 and 2043 cm⁻¹, respectively. The relatively small shift in ν(CO) [Δν(CO)] of ca. 30 cm⁻¹, as also observed on oxidation of [RuCl(CO)₂(PPh₃)(*o*-O₂C₆Cl₄)]⁻ and [Ru(CO)₂(PPh₃)₂(*o*-O₂C₆Cl₄)]³ for example, is consistent with catecholate- rather than metal-based oxidation {*cf.* the one-electron oxidation of *trans*-[Mn(CN)(CO)(dppm)]¹¹ to *trans*-[Mn(CN)(CO)(dppm)]⁺ ⁶ for which Δν(CO) = 74 cm⁻¹}.

Simulation of the well-resolved isotropic ESR spectra of [Ru(CN)(CO)₂(PPh₃)(*o*-O₂C₆Cl₄)] **1** and [Ru(CN)(CO)₂-(P(OPh)₃)(*o*-O₂C₆Cl₄)] **2** (Fig. 3) shows not only hyperfine coupling to the phosphorus atoms {*A*(³¹P) = *ca.* 20 and 25 G respectively} but also to two Cl atoms of the semiquinone ligand (Table 4). Satellites due to *ca.* 3 G coupling to ⁹⁹Ru and ¹⁰¹Ru (*I* = 5/2) are also observed. The *g*_{iso} values are close to that of the uncomplexed semiquinone anion radical (*o*-O₂C₆Cl₄)⁻ (*g*_{iso} = 2.0053).¹²

The synthesis and characterisation of

[NEt₄][(*o*-O₂C₆Cl₄)L(OC)₂Ru(μ-CN)Ru(CO)₂L'(*o*-O₂C₆Cl₄)]

The bridge-cleavage reactions of the dimers [{Ru(CO)₂L(μ-*o*-O₂C₆Cl₄)₂] {L = PPh₃ or P(OPh)₃} with two equivalents of the cyanide complexes [NEt₄][Ru(CN)(CO)₂L(*o*-O₂C₆Cl₄)] {L = PPh₃ or P(OPh)₃} in CH₂Cl₂ gave yellow solutions to which

Table 4 IR and ESR spectroscopic data for semiquinone ruthenium complexes

Complex	IR/cm ⁻¹ ^a		<i>g</i> _{iso}	ESR	
	ν(CN)	ν(CO)		<i>A</i> (³¹ P) ^b /G	<i>A</i> (^{35,37} Cl) ^c /G
[Ru(CN)(CO) ₂ (PPh ₃)(<i>o</i> -O ₂ C ₆ Cl ₄)] 1	2138w	2077, 2023	2.0018	19.85	0.55
[Ru(CN)(CO) ₂ {P(OPh) ₃ }(<i>o</i> -O ₂ C ₆ Cl ₄)] 2	2142w	2093, 2043	2.0030	25.08	0.60
[Ru(CO) ₂ (NCMe)(PPh ₃)(<i>o</i> -O ₂ C ₆ Cl ₄)] ⁺	—	2092, 2040	2.0029	5.00 ^d	^e
[Ru(CO) ₂ {P(OPh) ₃ }(<i>o</i> -O ₂ C ₆ Cl ₄)] ⁺	—	2102, 2056	2.0003	25.67 ^f	0.70
[Ru(CO) ₂ (PPh ₃) ₂ (<i>o</i> -O ₂ C ₆ Cl ₄)] ⁺	—	2073, 2021	2.0016	25.05 ^f	0.55
[Ru(CO) ₂ {P(OPh) ₃ }(PPh ₃)(<i>o</i> -O ₂ C ₆ Cl ₄)] ⁺	—	2089, 2040	2.0027	35.25, 18.15 ^g	0.60
[(<i>o</i> -O ₂ C ₆ Cl ₄)(Ph ₃ P)(OC) ₂ Ru(μ-CN)Ru(CO) ₂ (PPh ₃)(<i>o</i> -O ₂ C ₆ Cl ₄)] 8	^h	^h	2.0023	13.65	2.4
[(<i>o</i> -O ₂ C ₆ Cl ₄)(Ph ₃ P)(OC) ₂ Ru(μ-CN)Ru(CO) ₂ {P(OPh) ₃ }(<i>o</i> -O ₂ C ₆ Cl ₄)] 9	^h	^h	2.0034	15.85	3.0
[(<i>o</i> -O ₂ C ₆ Cl ₄)(PhO) ₃ P](OC) ₂ Ru(μ-CN)Ru(CO) ₂ {P(OPh) ₃ }(<i>o</i> -O ₂ C ₆ Cl ₄)] 10	^h	^h	2.0024	16.55	2.3
[(<i>o</i> -O ₂ C ₆ Cl ₄)(PhO) ₃ P](OC) ₂ Ru(μ-CN)Ru(CO) ₂ {PPh ₃ }(<i>o</i> -O ₂ C ₆ Cl ₄)] 11	^h	^h	2.0032	6.70 ⁱ	3.0

^a Strong absorptions in CH₂Cl₂ unless otherwise stated; w = weak. ^b 1 : 1 doublets unless otherwise stated. ^c Coupling to two chlorine atoms. ^d See text for description of multiplicity. *A*(¹⁴N) = 2.5 G also simulated. ^e Coupling to ^{35,37}Cl not resolved. ^f 1 : 2 : 1 triplet. ^g Doublet of doublets. ^h See Table 8. ⁱ See text for description of multiplicity. *A*(¹⁴N) = 4.5 G also simulated.

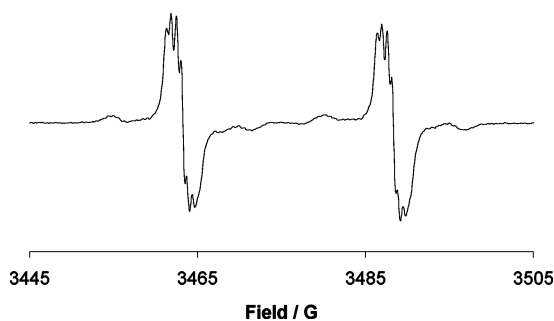


Fig. 3 The ESR spectrum of $[\text{Ru}(\text{CN})(\text{CO})_2\{\text{P}(\text{OPh})_3\}(o\text{-O}_2\text{C}_6\text{Cl}_4)] \mathbf{2}$ generated by reacting $[\text{NEt}_4]^{2-}$ with $[\text{Fe}(\eta\text{-C}_5\text{H}_4\text{COMe})(\eta\text{-C}_5\text{H}_5)][\text{BF}_4]$ in CH_2Cl_2 at 294 K.

n-hexane was added to precipitate the yellow solids $[\text{NEt}_4][(\text{o-O}_2\text{C}_6\text{Cl}_4)\text{L}(\text{OC})_2\text{Ru}(\mu\text{-CN})\text{Ru}(\text{CO})_2\text{L}'(o\text{-O}_2\text{C}_6\text{Cl}_4)]$ $\{\text{L} = \text{L}' = \text{PPh}_3, [\text{NEt}_4]^+\mathbf{8}^-; \text{L} = \text{PPh}_3, \text{L}' = \text{P}(\text{OPh})_3, [\text{NEt}_4]^+\mathbf{9}^-; \text{L} = \text{L}' = \text{P}(\text{OPh})_3, [\text{NEt}_4]^+\mathbf{10}^-; \text{L} = \text{P}(\text{OPh})_3, \text{L}' = \text{PPh}_3, [\text{NEt}_4]^+\mathbf{11}^-\}$. The salts, which include the linkage isomers $[\text{NEt}_4]^+\mathbf{9}^-$ and $[\text{NEt}_4]^+\mathbf{11}^-$, were characterised by elemental analysis and IR and ^{31}P NMR spectroscopy (Table 5).

The $\nu(\text{CN})$ bands of $\mathbf{8}^-$ – $\mathbf{11}^-$ occur at higher energy than those of $[\text{NEt}_4][\text{Ru}(\text{CN})(\text{CO})_2\text{L}(o\text{-O}_2\text{C}_6\text{Cl}_4)]$ $\{\text{L} = \text{PPh}_3, [\text{NEt}_4]^+\mathbf{1}^-$ or $\text{P}(\text{OPh})_3, [\text{NEt}_4]^+\mathbf{2}^-\}$, as expected from the kinematic effect¹³ of restricting the CN motion by *N*-coordination to the second metal fragment. The two dicarbonyl groups of $\mathbf{10}^-$ give rise, coincidentally, to only two broad $\nu(\text{CO})$ bands, at 2075 and 2016 cm^{-1} ; the remaining three anions, $\mathbf{8}^-$, $\mathbf{9}^-$ and $\mathbf{11}^-$ each show four bands. For $\mathbf{9}^-$ the bands at 2074 and 2014 cm^{-1} can be unambiguously assigned to the $\text{Ru}(\text{CO})_2\{\text{P}(\text{OPh})_3\}$ group and those at 2055 and 1995 cm^{-1} to the $\text{Ru}(\text{CO})_2(\text{PPh}_3)$ group. (A similar assignment can be made for $\mathbf{11}^-$.) The IR carbonyl spectrum of $\mathbf{8}^-$ is less easily assigned. However, the bands at 2050 and 1986 cm^{-1} are assigned to the *C*-bound $\text{Ru}(\text{CO})_2$ group by comparison with those of $[\text{NEt}_4][\text{Ru}(\text{CN})(\text{CO})_2(\text{PPh}_3)(o\text{-O}_2\text{C}_6\text{Cl}_4)]$ $[\text{NEt}_4]^+\mathbf{1}^-$ (2047 and 1983 cm^{-1}), and the bands at 2058 and 1995 cm^{-1} are assigned to the *N*-bound $\text{Ru}(\text{CO})_2$ group by comparison with those of $[\text{Ru}(\text{CO})_2(\text{NCMe})(\text{PPh}_3)(o\text{-O}_2\text{C}_6\text{Cl}_4)]$ (2056 and 1992 cm^{-1}). Notably there is very little difference between the carbonyl spectra of the linkage isomers $\mathbf{9}^-$ and $\mathbf{11}^-$.

Each of the ^{31}P NMR spectra of $\mathbf{8}^-$ – $\mathbf{11}^-$ shows two doublets (*J ca.* 10–20 Hz) due to phosphorus–phosphorus coupling through the P-Ru-CN-Ru-P skeleton. For $\mathbf{8}^-$ the signal at δ 20.4 is assigned to the PPh_3 ligand of the *C*-bound ruthenium fragment $\{\text{cf. } [\text{NEt}_4][\text{Ru}(\text{CN})(\text{CO})_2(\text{PPh}_3)(o\text{-O}_2\text{C}_6\text{Cl}_4)]$ $[\text{NEt}_4]^+\mathbf{1}^-$, δ 19.7} while that at δ 36.9 is assigned to PPh_3 of the *N*-bound ruthenium group. The spectrum of $[\text{NEt}_4]^+\mathbf{10}^-$ shows one signal at δ 110.5 assigned to the $\text{P}(\text{OPh})_3$ -bound NC-Ru group and another at δ 114.3 assigned to $\text{P}(\text{OPh})_3$ of the *N*-bound ruthenium fragment. Replacing the PPh_3 of the *N*-bound ruthenium fragment of $[\text{NEt}_4]^+\mathbf{8}^-$ with $\text{P}(\text{OPh})_3$, to give $[\text{NEt}_4]^+\mathbf{9}^-$, results in signals at δ 20.4 and 114.6, the latter due to the phosphite ligand. The linkage isomer $[\text{NEt}_4]^+\mathbf{11}^-$ is therefore readily distinguished from $[\text{NEt}_4]^+\mathbf{9}^-$ by ^{31}P NMR spectroscopy (but not by the IR carbonyl spectrum, as noted above) since it shows signals at δ 37.1 and 110.9.

Table 5 Analytical and IR and ^{31}P NMR spectroscopic data for $[\text{NEt}_4][(\text{o-O}_2\text{C}_6\text{Cl}_4)\text{L}(\text{OC})_2\text{Ru}(\mu\text{-CN})\text{Ru}(\text{CO})_2\text{L}'(o\text{-O}_2\text{C}_6\text{Cl}_4)]$

Complex ^a	L	L'	Colour	Yield (%)	Analysis (%) ^b				IR/ cm^{-1c}		^{31}P NMR (ppm)
					C	H	N		$\nu(\text{CN})$	$\nu(\text{CO})$	
$\mathbf{8}^-$	PPh_3	PPh_3	Yellow	66	49.3 (49.3)	3.6 (3.4)	2.0 (1.9)	2155w	2058ms, 2050, 1995ms, 1986	20.4 (d, J_{pp} 12, NC-Ru-PPh ₃), 36.9 (d, J_{pp} 12, CN-Ru-PPh ₃)	
$\mathbf{9}^-$	PPh_3	$\text{P}(\text{OPh})_3$	Yellow	76	48.3 (48.3)	3.5 (3.7)	2.0 (1.8)	2156w	2074, 2055ms, 2014, 1995ms	20.4 (d, J_{pp} 15, NC-Ru-PPh ₃), 114.6 {d, J_{pp} 15, CN-Ru-P(OPh) ₃ }	
$\mathbf{10}^-$	$\text{P}(\text{OPh})_3$	$\text{P}(\text{OPh})_3$	Yellow	73	45.7 (45.9)	3.0 (3.2)	1.4 (1.8)	2162w	2075s, brd, 2016s, brd	110.5 {d, J_{pp} 21, NC-Ru-P(OPh) ₃ }, 114.3 {d, J_{pp} 21, CN-Ru-P(OPh) ₃ }	
$\mathbf{11}^-$	$\text{P}(\text{OPh})_3$	PPh_3	Yellow	66	47.6 (47.3)	3.5 (3.3)	2.0 (1.8)	2158w	2071, 2057ms, 2013, 1997ms	37.1 (d, J_{pp} 15, C-NRu-PPh ₃), 110.9 {d, J_{pp} 15, NC-Ru-P(OPh) ₃ }	

^a $[\text{NEt}_4]^+$ salts. ^b Calculated values in parentheses. ^c Strong (s) absorptions in CH_2Cl_2 unless otherwise stated; w = weak, m = medium, brd = broad. ^d Calculated as a 2 : 1 *n*-hexane solvate.

Table 6 Selected bond lengths (Å) and angles (°) for $[(o\text{-O}_2\text{C}_6\text{Cl}_4)(\text{Ph}_3\text{P})(\text{OC})_2\text{Ru}(\mu\text{-CN})\text{Ru}(\text{CO})_2(\text{PPh}_3)(o\text{-O}_2\text{C}_6\text{Cl}_4)]$ **8** and $[(o\text{-O}_2\text{C}_6\text{Cl}_4)(\text{Ph}_3\text{P})(\text{OC})_2\text{Ru}(\mu\text{-CN})\text{Ru}(\text{CO})_2(\text{PPh}_3)(o\text{-O}_2\text{C}_6\text{Cl}_4)]^-$ **8⁻**

	8	8⁻		8	8⁻
C(25)–N(1)	1.127(7)	1.132(4)	C(26)–Ru(1)–P(1)	94.67(18)	95.61(10)
C(25)–Ru(1)	2.087(8)	2.114(3)	C(27)–Ru(1)–P(1)	87.41(19)	88.74(10)
P(1)–Ru(1)	2.385(2)	2.365(1)	C(25)–Ru(1)–P(1)	173.53(15)	175.57(8)
C(26)–Ru(1)	1.878(7)	1.886(4)	O(1)–Ru(1)–O(2)	80.24(16)	81.12(8)
C(27)–Ru(1)	1.867(7)	1.889(3)	C(26)–Ru(1)–O(1)	174.3(2)	172.15(12)
O(1)–Ru(1)	2.073(4)	2.071(2)	C(27)–Ru(1)–O(2)	176.8(2)	177.76(11)
O(2)–Ru(1)	2.078(4)	2.070(2)	C(26)–Ru(1)–O(2)	94.7(2)	91.15(12)
P(1')–Ru(1')	2.393(2)	2.361(8)	C(27)–Ru(1)–O(1)	96.5(2)	97.95(12)
C(26')–Ru(1')	1.888(7)	1.887(3)	P(1)–Ru(1)–O(1)	88.21(12)	86.25(6)
C(27')–Ru(1')	1.893(7)	1.884(3)	P(1)–Ru(1)–O(2)	92.65(12)	93.22(6)
O(1')–Ru(1')	2.072(4)	2.074(2)	C(26)–Ru(1)–C(27)	88.5(3)	89.73(14)
O(2')–Ru(1')	2.088(4)	2.067(2)	C(26')–Ru(1')–P(1')	93.59(19)	90.90(10)
N(1)–Ru(1)	2.083(8)	2.129(3)	C(27')–Ru(1')–P(1')	91.93(19)	93.80(10)
C(19)–O(1)	1.334(7)	1.326(4)	N(1')–Ru(1')–P(1')	171.05(16)	177.64(8)
C(24)–O(2)	1.311(7)	1.325(4)	O(1')–Ru(1')–O(2')	79.24(15)	80.61(8)
C(19')–O(1')	1.293(7)	1.324(4)	C(26')–Ru(1')–O(1')	174.9(2)	174.35(11)
C(24')–O(2')	1.296(7)	1.328(4)	C(27')–Ru(1')–O(2')	173.6(2)	174.02(11)
C(19)–C(20)	1.397(8)	1.395(4)	C(26')–Ru(1')–O(2')	95.7(2)	94.61(11)
C(20)–C(21)	1.372(9)	1.401(4)	C(27')–Ru(1')–O(1')	95.4(2)	93.45(11)
C(21)–C(22)	1.392(9)	1.387(5)	P(1')–Ru(1')–O(1')	85.91(12)	91.85(6)
C(22)–C(23)	1.391(8)	1.392(5)	P(1')–Ru(1')–O(2')	91.16(12)	87.09(6)
C(23)–C(24)	1.416(8)	1.392(4)	C(26')–Ru(1')–C(27')	89.7(3)	91.29(14)
C(19)–C(24)	1.428(8)	1.419(5)	Ru(1)–C(25)–N(1)	172.0(5)	164.1(3)
C(19')–C(20')	1.406(8)	1.389(4)	C(25)–N(1)–Ru(1')	169.6(5)	156.3(3)
C(20')–C(21')	1.366(9)	1.402(4)			
C(21')–C(22')	1.439(9)	1.385(5)			
C(22')–C(23')	1.361(8)	1.397(4)			
C(23')–C(24')	1.404(8)	1.390(4)			
C(19')–C(24')	1.455(8)	1.426(4)			

The X-ray structure of the anion of $[\text{NET}_4][[(o\text{-O}_2\text{C}_6\text{Cl}_4)(\text{Ph}_3\text{P})(\text{OC})_2\text{Ru}(\mu\text{-CN})\text{Ru}(\text{CO})_2(\text{PPh}_3)(o\text{-O}_2\text{C}_6\text{Cl}_4)]^-]$ **8⁻** is shown in Fig. 4(a) and selected bond lengths and angles are given in Table 6. Crystallographic refinement revealed that the bridging cyanide unit is disordered equally over the two possible orientations.

The geometry at both ruthenium centres of **8⁻** is approximately octahedral. Each metal is bonded to two *cis* CO ligands *trans* to a chelating *o*-O₂C₆Cl₄ ligand, to a PPh₃ ligand and to a bridging cyanide. The cyanide bridge is bent; the two angles of the Ru–C–N–Ru skeleton are 164.1(3) and 156.3(3)°, smaller than found in $[(o\text{-O}_2\text{C}_6\text{Cl}_4)(\text{Ph}_3\text{P})(\text{OC})_2\text{Ru}(\mu\text{-CN})\text{Mn}(\text{CO})_2(\text{PEt}_3)(\text{dppe})\text{-}cis]$ {Mn–C–N = 174.8(5) and Ru–N–C = 171.4(4)°}.⁶ The C–C distances in the *o*-O₂C₆Cl₄ ligands and the C–O distances (1.32–1.33 Å) in the metal–chelate rings are similar to those of $[\text{NET}_4][\text{Ru}(\text{CN})(\text{CO})_2(\text{PPh}_3)(o\text{-O}_2\text{C}_6\text{Cl}_4)]^-$ **1⁻**, again consistent with the presence of catecholate ligands. The bending at the bridging cyanide ligand is such that although the two catecholate ligands lie on the same side of the molecule they are bent away from each other (the angle between their mean planes is 45°); the $[\text{NET}_4]^+$ cation {not shown in Fig. 4(a)} lies in the space between them.

The CVs of **8⁻**–**11⁻** (Table 7) show two reversible oxidation waves (*cf.* the irreversibility of the second oxidation wave of the mononuclear cyanide complexes **1⁻** and **2⁻**) in the ranges 0.42–0.52 and 0.60–0.70 V, corresponding to the sequential formation of the neutral complexes $[(o\text{-O}_2\text{C}_6\text{Cl}_4)\text{L}(\text{OC})_2\text{Ru}(\mu\text{-CN})\text{Ru}(\text{CO})_2\text{L}'(o\text{-O}_2\text{C}_6\text{Cl}_4)]$ {L = L' = PPh₃, **8**; L = PPh₃, L' = P(OPh)₃, **9**; L = L' = P(OPh)₃, **10**; L = P(OPh)₃, L' = PPh₃, **11⁺**}.

Table 7 Electrochemical data for the oxidation of $[\text{NET}_4][[(o\text{-O}_2\text{C}_6\text{Cl}_4)\text{L}(\text{OC})_2\text{Ru}(\mu\text{-CN})\text{Ru}(\text{CO})_2\text{L}'(o\text{-O}_2\text{C}_6\text{Cl}_4)]^-]$

Complex	L	L'	E_o^a/V	
			$z = -1 \rightarrow 0$	$z = 0 \rightarrow +1$
1⁻	PPh ₃	PPh ₃	0.42	0.60
2⁻	PPh ₃	P(OPh) ₃	0.44	0.68
3⁻	P(OPh) ₃	P(OPh) ₃	0.52	0.70
4⁻	P(OPh) ₃	PPh ₃	0.44	0.68

^a Potentials calibrated vs. the $[\text{Fe}(\eta\text{-C}_5\text{Me}_5)_2]^+ / [\text{Fe}(\eta\text{-C}_5\text{Me}_5)_2]$ couple (at –0.08 V).

11⁺ and the cations $[(o\text{-O}_2\text{C}_6\text{Cl}_4)\text{L}(\text{OC})_2\text{Ru}(\mu\text{-CN})\text{Ru}(\text{CO})_2\text{L}'(o\text{-O}_2\text{C}_6\text{Cl}_4)]^+$ {L = L' = PPh₃, **8⁺**; L = PPh₃, L' = P(OPh)₃, **9⁺**; L = L' = P(OPh)₃, **10⁺**; L = P(OPh)₃, L' = PPh₃, **11⁺**}. The small separation, *ca.* 200 mV, between the two oxidation waves compares with the much larger separation of *ca.* 1.1 V for the mononuclear anions $[\text{Ru}(\text{CN})(\text{CO})_2(\text{PPh}_3)(o\text{-O}_2\text{C}_6\text{Cl}_4)]^-$ **1⁻** and $[\text{Ru}(\text{CN})(\text{CO})_2\{\text{P}(\text{OPh})_3\}(o\text{-O}_2\text{C}_6\text{Cl}_4)]^-$ **2⁻** and is therefore more consistent with sequential oxidation of each of the two catecholate ligands to semiquinones rather than formation of a quinone ligand by overall two-electron oxidation at one Ru(CO)₂(*o*-O₂C₆Cl₄) centre.

The site of first oxidation of **8⁻**–**11⁻** (*i.e.* at the *N*- or *C*-bound end of the cyanide bridge) can be tentatively assigned on the basis of the relative dependence of the two oxidation potentials on L and L', coupled with the assignment of first oxidation at the *C*-bound centre of **8⁻** from the X-ray structural determination of

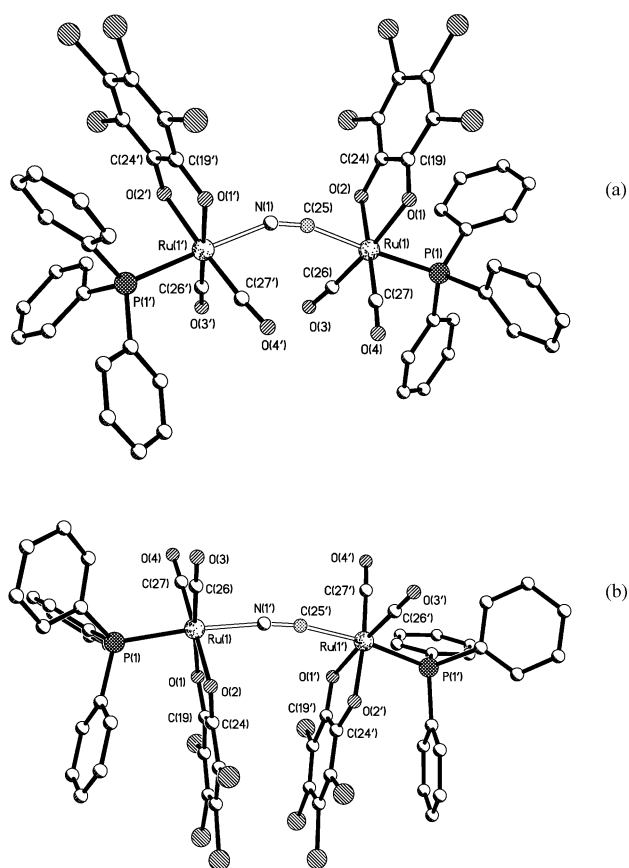


Fig. 4 The structures of (a) the anion $\mathbf{8}^-$, and (b) the neutral molecule $\mathbf{8}$. Hydrogen atoms have been omitted for clarity. The structure of $\mathbf{8}^-$ has the CN bridge equally divided between the two orientations. The cyanide bridge in $\mathbf{8}$ is shown in the major orientation (65%); the C and N atom positions are reversed in the remaining 35%. In both cases the two ends of the molecule are crystallographically independent; the carbon atoms of the six-membered rings of the $\text{O}_2\text{C}_6\text{Cl}_4$ ligands are numbered from C(19) to C(24) and from C(19') to C(24').

$\mathbf{8}$ (see below). First, $\mathbf{10}^-$, with $\text{L} = \text{L}' = \text{P}(\text{OPh})_3$, is reasonably assumed also to oxidise first at the *C*-bound centre as its two oxidation waves (at 0.52 and 0.70 V) are both shifted to more positive potentials, by *ca.* 100 mV, from those of $[\text{NET}_4]^+\mathbf{8}^-$ (with $\text{L} = \text{L}' = \text{PPh}_3$); a similar shift occurs when the PPh_3 ligand of $\mathbf{1}^-$ is replaced by $\text{P}(\text{OPh})_3$ to give $\mathbf{2}^-$. Next, when $\text{L}' = \text{PPh}_3$ is replaced in $\mathbf{8}^-$ by $\text{P}(\text{OPh})_3$, to give $\mathbf{9}^-$, the first oxidation potential is virtually unchanged, again consistent with oxidation at the *C*-bound centre. However, when $\text{L} = \text{PPh}_3$ is replaced in $\mathbf{8}^-$ by $\text{P}(\text{OPh})_3$, to give $\mathbf{11}^-$, the invariance of the first oxidation potential suggests that the site of oxidation also changes; in this case, uniquely among the four binuclear anions, oxidation occurs first at the *N*-bound centre. {The same deduction results from a consideration of the 80 mV negative shift in the first potential when $\text{L}' = \text{P}(\text{OPh})_3$ in $\mathbf{10}^-$ is replaced by PPh_3 , to give $\mathbf{11}^-$.} Overall, however, the dependence of oxidation potential on L , L' and the cyanide bridge orientation in $[(o\text{-O}_2\text{C}_6\text{Cl}_4)\text{L}(\text{OC})_2\text{Ru}(\mu\text{-CN})\text{Ru}(\text{CO})_2\text{L}'(o\text{-O}_2\text{C}_6\text{Cl}_4)]^-$ does not allow a distinction to be made between the linkage isomers $\mathbf{9}^-$ and $\mathbf{11}^-$, which have identical first and second oxidation potentials.

The synthesis and characterisation of $[(o\text{-O}_2\text{C}_6\text{Cl}_4)\text{L}(\text{OC})_2\text{Ru}(\mu\text{-CN})\text{Ru}(\text{CO})_2\text{L}'(o\text{-O}_2\text{C}_6\text{Cl}_4)]^-$ and $[(o\text{-O}_2\text{C}_6\text{Cl}_4)\text{L}(\text{OC})_2\text{Ru}(\mu\text{-CN})\text{Ru}(\text{CO})_2\text{L}'(o\text{-O}_2\text{C}_6\text{Cl}_4)]^+[\text{BF}_4]^-$

Unlike the mononuclear cyanide complexes $[\text{NET}_4][\text{Ru}(\text{CN})(\text{CO})_2\text{L}(o\text{-O}_2\text{C}_6\text{Cl}_4)]$ $\{\text{L} = \text{PPh}_3, [\text{NET}_4]^+\mathbf{1}^-$ or $\text{P}(\text{OPh})_3, [\text{NET}_4]^+\mathbf{2}^-\}$, where only the first oxidation occurs at chemically accessible potentials, the electrochemical data for $\mathbf{8}^-$ – $\mathbf{11}^-$ suggested that both the neutral complexes $[(o\text{-O}_2\text{C}_6\text{Cl}_4)\text{L}(\text{OC})_2\text{Ru}(\mu\text{-CN})\text{Ru}(\text{CO})_2\text{L}'(o\text{-O}_2\text{C}_6\text{Cl}_4)]$ and the monocations $[(o\text{-O}_2\text{C}_6\text{Cl}_4)\text{L}(\text{OC})_2\text{Ru}(\mu\text{-CN})\text{Ru}(\text{CO})_2\text{L}'(o\text{-O}_2\text{C}_6\text{Cl}_4)]^+$ might be isolable.

Accordingly, the purple salts $[(o\text{-O}_2\text{C}_6\text{Cl}_4)\text{L}(\text{OC})_2\text{Ru}(\mu\text{-CN})\text{Ru}(\text{CO})_2\text{L}'(o\text{-O}_2\text{C}_6\text{Cl}_4)]^+[\text{BF}_4]^-$ $\{\text{L} = \text{L}' = \text{PPh}_3, \mathbf{8}^+[\text{BF}_4]^-$; $\text{L} = \text{PPh}_3, \text{L}' = \text{P}(\text{OPh})_3, \mathbf{9}^+[\text{BF}_4]^-$; $\text{L} = \text{L}' = \text{P}(\text{OPh})_3, \mathbf{10}^+[\text{BF}_4]^-$; $\text{L} = \text{P}(\text{OPh})_3, \text{L}' = \text{PPh}_3, \mathbf{11}^+[\text{BF}_4]^-$ were prepared in good yields by reacting $[\text{NET}_4][(o\text{-O}_2\text{C}_6\text{Cl}_4)\text{L}(\text{OC})_2\text{Ru}(\mu\text{-CN})\text{Ru}(\text{CO})_2\text{L}'(o\text{-O}_2\text{C}_6\text{Cl}_4)]$ $\{\text{L} = \text{L}' = \text{PPh}_3$ or $\text{P}(\text{OPh})_3\}$ with two equivalents of $[\text{Fe}(\eta\text{-C}_5\text{H}_4\text{COME})(\eta\text{-C}_5\text{H}_5)]^+[\text{BF}_4]^-$ in CH_2Cl_2 .

The neutral complexes $[(o\text{-O}_2\text{C}_6\text{Cl}_4)\text{L}(\text{OC})_2\text{Ru}(\mu\text{-CN})\text{Ru}(\text{CO})_2\text{L}'(o\text{-O}_2\text{C}_6\text{Cl}_4)]$ $\{\text{L} = \text{L}' = \text{PPh}_3, \mathbf{8}$ or $\text{P}(\text{OPh})_3, \mathbf{10}\}$ were similarly prepared, as red solids, by reacting $[\text{NET}_4][(o\text{-O}_2\text{C}_6\text{Cl}_4)\text{L}(\text{OC})_2\text{Ru}(\mu\text{-CN})\text{Ru}(\text{CO})_2\text{L}'(o\text{-O}_2\text{C}_6\text{Cl}_4)]$ $\{\text{L} = \text{L}' = \text{PPh}_3, [\text{NET}_4]^+\mathbf{8}^-$; $\text{L} = \text{L}' = \text{P}(\text{OPh})_3, [\text{NET}_4]^+\mathbf{10}^-$ with one equivalent of $[\text{Fe}(\eta\text{-C}_5\text{H}_4\text{COME})(\eta\text{-C}_5\text{H}_5)]^+[\text{BF}_4]^-$. However, the analogous complexes $[(o\text{-O}_2\text{C}_6\text{Cl}_4)\text{L}(\text{OC})_2\text{Ru}(\mu\text{-CN})\text{Ru}(\text{CO})_2\text{L}'(o\text{-O}_2\text{C}_6\text{Cl}_4)]$ $\{\text{L} = \text{PPh}_3, \text{L}' = \text{P}(\text{OPh})_3, \mathbf{9}$; $\text{L} = \text{P}(\text{OPh})_3, \text{L}' = \text{PPh}_3, \mathbf{11}\}$ were better prepared by the comproportionation reactions of $[\text{NET}_4]^+\mathbf{9}^-$ or $[\text{NET}_4]^+\mathbf{11}^-$ with $\mathbf{9}^+[\text{BF}_4]^-$ or $\mathbf{11}^+[\text{BF}_4]^-$.

Complexes $\mathbf{8}$ – $\mathbf{11}$ (soluble in solvents such as CH_2Cl_2 , diethyl ether and toluene but not in *n*-hexane) and $\mathbf{8}^+[\text{BF}_4]^-$ – $\mathbf{11}^+[\text{BF}_4]^-$ were characterised by elemental analysis, IR spectroscopy (Table 8), cyclic voltammetry (which showed two waves, one oxidation and one reduction for the neutral species, and two reductions for the cations, at potentials identical to those for the corresponding anions), ESR spectroscopy and, for $\mathbf{8}$ and $\mathbf{9}$ (but see below), by X-ray crystallography.

The IR spectra of $\mathbf{8}$ and $\mathbf{10}$ each show four carbonyl bands, two of which are shifted to higher energy (by *ca.* 20–30 cm^{-1} , as found for the oxidation of $[\text{Ru}(\text{CN})(\text{CO})_2\text{L}(o\text{-O}_2\text{C}_6\text{Cl}_4)]^-$ to $[\text{Ru}(\text{CN})(\text{CO})_2\text{L}(o\text{-O}_2\text{C}_6\text{Cl}_4)]$) by comparison with those of the anions $\mathbf{8}^-$ and $\mathbf{10}^-$ while the other two are shifted to higher energy by only *ca.* 5 cm^{-1} . Thus, one catechol ligand is oxidised to a semiquinone. Similar behaviour was observed on oxidation of $\mathbf{9}^-$ and $\mathbf{11}^-$ although the shifts to higher energy result in the observation of only two broad carbonyl bands for $\mathbf{9}$ and $\mathbf{11}$. On further oxidation, similar shifts on formation of the second $\text{Ru}(\text{CO})_2(\text{semiquinone})$ fragment result in coincident bands for each of $\mathbf{8}^+$ and $\mathbf{10}^+$ but a set of four resolved bands for $\mathbf{9}^+$ and $\mathbf{11}^+$. The IR spectral changes observed on stepwise oxidation of $\mathbf{8}^-$ to $\mathbf{8}$ and $\mathbf{8}^+$ are shown in Fig. 5

On oxidation of $\mathbf{8}^-$ and $\mathbf{10}^-$ the cyanide band shifts to higher energy by *ca.* 30 cm^{-1} (*cf.* 10 cm^{-1} for the mononuclear anions) but on formation of $\mathbf{8}^+$ and $\mathbf{10}^+$ this band shifts to lower energy, by *ca.* 4 cm^{-1} . Such shifts are consistent with sequential oxidation at the *C*-bound and *N*-bound $\text{Ru}(\text{CO})_2(o\text{-O}_2\text{C}_6\text{Cl}_4)$ fragments, as deduced above for $\mathbf{8}^-$, $\mathbf{9}^-$ and $\mathbf{10}^-$. (Unfortunately, the cyanide bands of $\mathbf{9}$ and $\mathbf{11}$ were not detected so that first oxidation at the *N*-bound $\text{Ru}(\text{CO})_2(o\text{-O}_2\text{C}_6\text{Cl}_4)$ group of $\mathbf{11}^-$ could not be confirmed.) Similar shifts, of –15 and 31 cm^{-1} respectively, are observed for

Table 8 Analytical and IR spectroscopic data for $[(o\text{-O}_2\text{C}_6\text{Cl}_4)\text{L}(\text{OC})_2\text{Ru}(\mu\text{-CN})\text{Ru}(\text{CO})_2\text{L}'(o\text{-O}_2\text{C}_6\text{Cl}_4)]$ and $[(o\text{-O}_2\text{C}_6\text{Cl}_4)\text{L}(\text{OC})_2\text{Ru}(\mu\text{-CN})\text{Ru}(\text{CO})_2\text{L}'(o\text{-O}_2\text{C}_6\text{Cl}_4)][\text{BF}_4]$

Complex	L	L'	Colour	Yield (%)	Analysis ^a (%)			IR ^b /cm ⁻¹	
					C	H	N	$\nu(\text{CN})$	$\nu(\text{CO})$
8^c	PPh ₃	PPh ₃	Red	51	45.7 (45.9)	2.7 (2.4)	1.0 (1.0)	2187w	2080, 2053, 2028, 1990
9^d	PPh ₃	P(OPh) ₃	Red	72	46.1 (46.0)	2.5 (2.6)	0.9 (1.0)	—	2082vs, 2028ms
10	P(OPh) ₃	P(OPh) ₃	Red	71	43.2 (43.4)	2.1 (2.1)	1.2 (1.0)	2185w	2099, 2072, 2050, 2013
11	P(OPh) ₃	PPh ₃	Red	85	45.1 (44.9)	2.1 (2.2)	1.0 (1.0)	—	2082vs, 2029ms
8⁺[BF₄]^{-e}	PPh ₃	PPh ₃	Purple	68	45.9 (45.9)	2.4 (2.3)	1.0 (1.0)	2183w	2087, 2035
9⁺[BF₄]^{-d}	PPh ₃	P(OPh) ₃	Purple	82	43.4 (43.4)	2.9 (2.5)	1.5 (0.9)	2184w	2104, 2085, 2054, 2034
10⁺[BF₄]^{-d}	P(OPh) ₃	P(OPh) ₃	Purple	66	41.1 (40.9)	2.1 (2.0)	1.0 (0.9)	2187w	2105, 2055
11⁺[BF₄]^{-d}	P(OPh) ₃	PPh ₃	Purple	62	43.6 (43.4)	2.6 (2.5)	1.3 (0.9)	2184w	2104, 2086, 2054, 2034

^a Calculated values in parentheses. ^b Strong (s) absorptions in CH₂Cl₂ unless otherwise stated; w = weak, m = medium, vs = very strong. ^c Calculated as a 1 : 2 CH₂Cl₂ solvate. ^d Calculated as a 2 : 1 *n*-hexane solvate. ^e Calculated as a 2 : 1 CH₂Cl₂ solvate.

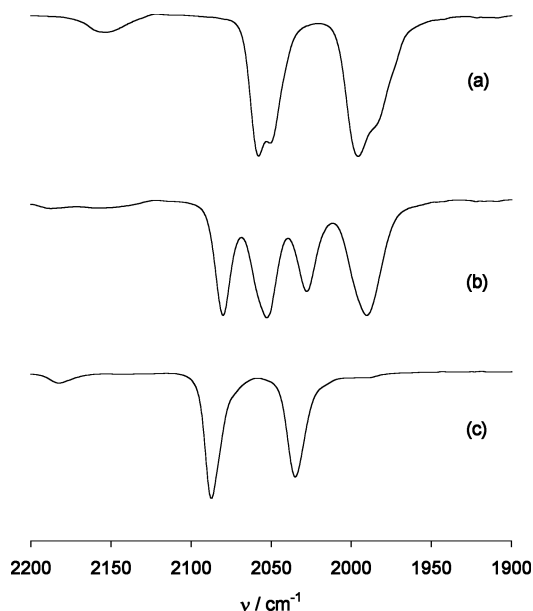


Fig. 5 IR spectra of $[(o\text{-O}_2\text{C}_6\text{Cl}_4)(\text{Ph}_3\text{P})(\text{OC})_2\text{Ru}(\mu\text{-CN})\text{Ru}(\text{CO})_2(\text{PPh}_3)(o\text{-O}_2\text{C}_6\text{Cl}_4)]^z$ (a) $z = -1$, **8⁻**; (b) $z = 0$, **8**; (c) $z = 1$, **8⁺**.

$[(o\text{-O}_2\text{C}_6\text{Cl}_4)\text{L}(\text{OC})_2\text{Ru}(\mu\text{-NC})\text{Mn}(\text{CO})_2\{\text{P}(\text{OPh})_3\}(\text{dppm})\text{-trans}]$ and $[(o\text{-O}_2\text{C}_6\text{Cl}_4)\text{L}(\text{OC})_2\text{Ru}(\mu\text{-NC})\text{Mn}(\text{CO})(\text{dppm})_2]$ when oxidised at the *N*-bound and *C*-bound redox centres.⁶

The ESR spectra of **8–11**, in CH₂Cl₂ at 294 K (Table 4), are similar to those of **1** and **2** in showing hyperfine coupling to the phosphorus atoms of PPh₃ or P(OPh)₃ and satellites due to coupling to ⁹⁹Ru and ¹⁰¹Ru. (Coupling to the ring chlorine atoms was not fully resolved though the line widths of the spectra of **9** and **11** were better simulated with the inclusion of small couplings to two such atoms—as observed for **1** and **2**). However, there is a marked difference between the spectrum of **11** and those of **8–10**. First, $A(^{31}\text{P})$ is much smaller (6.7 vs. ca. 14.0–17.0 G). Second, simulation of the spectrum of **11** revealed, uniquely, coupling to the nitrogen atom of the cyanide bridge $\{A(^{14}\text{N}) = 4.5 \text{ G}\}$. Thus, in agreement with the tentative assignment based on CV studies, complex **11⁻** is oxidised first at the *N*-bound $\text{Ru}(\text{CO})_2(o\text{-O}_2\text{C}_6\text{Cl}_4)$ fragment. [It is noteworthy that the ESR spectrum of $[\text{Ru}(\text{CO})_2(\text{NCMe})(\text{PPh}_3)(o\text{-O}_2\text{C}_6\text{Cl}_4)]^+$ (Table 4) also shows coupling to nitrogen $\{A(^{14}\text{N}) = 2.5 \text{ G}\}$ as well as a much smaller value of $A(^{31}\text{P})$, 5.0 G, compared with those of

$[\text{Ru}(\text{CO})_2\text{L}(\text{PPh}_3)(o\text{-O}_2\text{C}_6\text{Cl}_4)]^+$ $\{\text{L} = \text{PPh}_3 \text{ or } \text{P}(\text{OPh})_3\}$ (*i.e.* ca. 25.0 G).]

The cations **8⁺–11⁺**, containing two semiquinone ligands, show only ill-defined ESR spectra.

The molecular structures of $[(o\text{-O}_2\text{C}_6\text{Cl}_4)(\text{Ph}_3\text{P})(\text{OC})_2\text{Ru}(\mu\text{-CN})\text{Ru}(\text{CO})_2(\text{PPh}_3)(o\text{-O}_2\text{C}_6\text{Cl}_4)]$ **8** and $[(o\text{-O}_2\text{C}_6\text{Cl}_4)(\text{Ph}_3\text{P})(\text{OC})_2\text{Ru}(\mu\text{-CN})\text{Ru}(\text{CO})_2\{\text{P}(\text{OPh})_3\}(o\text{-O}_2\text{C}_6\text{Cl}_4)]$ **9A**

In order to define unequivocally the site of first oxidation in the binuclear anions $[(o\text{-O}_2\text{C}_6\text{Cl}_4)\text{L}(\text{OC})_2\text{Ru}(\mu\text{-CN})\text{Ru}(\text{CO})_2\text{L}'(o\text{-O}_2\text{C}_6\text{Cl}_4)]^-$ attempts were made to grow crystals of **8** and **9**. The structure of **8** has been determined successfully but single crystals obtained from **9** were found to be of an isomer, *i.e.* **9A**, with an unprecedented arrangement of the ligands in the $(\mu\text{-CN})\text{Ru}(\text{CO})_2\{\text{P}(\text{OPh})_3\}(o\text{-O}_2\text{C}_6\text{Cl}_4)$ unit.

The molecular structures of **8** and **9A** are shown in Fig. 4(b) and Fig. 6 respectively with selected bond lengths and angles given in Tables 6 (for **8**) and 9 (for **9A**). In **8**, as in **8⁻**, each approximately octahedral ruthenium centre is bonded to two *cis* CO ligands, a chelating *o*-O₂C₆Cl₄ ligand and a PPh₃ ligand *trans* to the cyanide bridge. However, in contrast to **8⁻**, the bond lengths in the two *o*-O₂C₆Cl₄ ligands of **8** are significantly different.

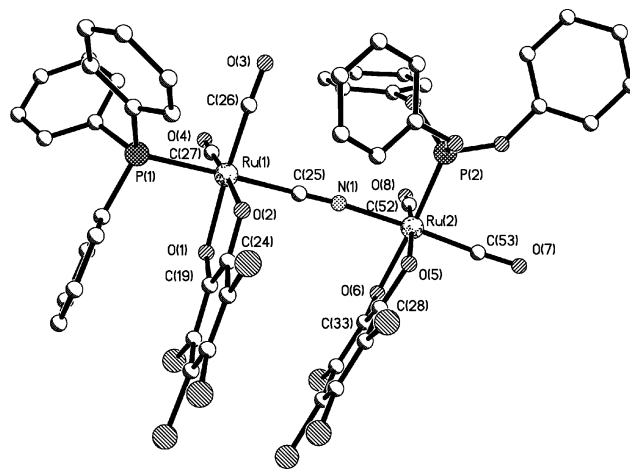


Fig. 6 The molecular structure of **9A**. Hydrogen atoms have been omitted for clarity. The carbon atoms of the six-membered rings of the two O₂C₆Cl₄ ligands are numbered from C(19) to C(24) and from C(28) to C(33).

Table 9 Selected bond lengths (Å) and angles (°) for [(*o*-O₂C₆Cl₄)(Ph₃P)(OC)₂Ru(μ-CN)Ru(CO)₂{P(OPh)₃}(*o*-O₂C₆Cl₄)] **9A**

C(25)–N(1)	1.147(12)	C(25)–Ru(1)–P(1)	177.4(3)
C(25)–Ru(1)	2.050(11)	C(27)–Ru(1)–P(1)	94.1(3)
P(1)–Ru(1)	2.430(3)	C(26)–Ru(1)–P(1)	89.5(3)
P(2)–Ru(2)	2.271(3)	O(1)–Ru(1)–O(2)	78.4(3)
C(26)–Ru(1)	1.901(11)	C(26)–Ru(1)–O(1)	174.0(4)
C(27)–Ru(1)	1.878(11)	C(27)–Ru(1)–O(2)	174.0(4)
O(1)–Ru(1)	2.091(7)	C(26)–Ru(1)–O(2)	95.9(4)
O(2)–Ru(1)	2.096(7)	C(27)–Ru(1)–O(1)	95.6(4)
C(52)–Ru(2)	1.872(12)	P(1)–Ru(1)–O(1)	92.09(19)
C(53)–Ru(2)	1.885(13)	P(1)–Ru(1)–O(2)	86.49(19)
O(5)–Ru(2)	2.055(8)	C(26)–Ru(1)–C(27)	90.1(5)
O(6)–Ru(2)	2.082(7)	N(1)–Ru(2)–P(2)	89.6(2)
N(1)–Ru(2)	2.102(9)	C(53)–Ru(2)–P(2)	90.1(4)
C(19)–O(1)	1.312(12)	C(52)–Ru(2)–P(2)	93.0(3)
C(24)–O(2)	1.296(12)	O(5)–Ru(2)–O(6)	81.6(3)
C(28)–O(5)	1.356(13)	C(52)–Ru(2)–O(5)	171.7(3)
C(33)–O(6)	1.323(13)	C(52)–Ru(2)–O(6)	90.2(4)
C(19)–C(20)	1.403(15)	C(53)–Ru(2)–O(5)	90.1(4)
C(20)–C(21)	1.356(15)	C(53)–Ru(2)–O(6)	94.4(4)
C(21)–C(22)	1.451(12)	P(2)–Ru(2)–O(5)	95.1(2)
C(22)–C(23)	1.370(15)	P(2)–Ru(2)–O(6)	174.4(2)
C(23)–C(24)	1.421(14)	C(52)–Ru(2)–C(53)	91.9(5)
C(19)–C(24)	1.461(11)		

Although crystallographic refinement indicated orientational disorder of the cyanide bridge in a 65(7) : 35(7) ratio, the structural parameters associated with the two Ru(CO)₂(PPh₃)(*o*-O₂C₆Cl₄) fragments are well enough defined to allow a distinction between catecholate and semiquinone forms of the chelating ligands. Thus, the C–O bond distances {C(19)–O(1) = 1.293(7) and C(24)–O(2) = 1.296(7) Å} of the *o*-O₂C₆Cl₄ ligand at the (majority) *C*-bound end of the cyanide bridge in **8** are consistent with a semiquinone {*cf.* the similar values of [Ru(CO)₂(PPh₃)₂(*o*-O₂C₆Cl₄)]⁺,⁹ [Ru(CO)₂(*o*-O₂C₆Cl₄)]₂,¹⁴ [RuCl₂(PPh₃)₂(*o*-O₂C₆H₃Cl)]¹⁵ and [Ru(CO)(trpy){*o*-O₂C₆H₂Bu₂}]⁺ (trpy = 2,2':6',2''-terpyridine)¹⁶}. Furthermore, the C(20)–C(21) and C(22)–C(23) bond lengths of 1.366(9) and 1.361(8) Å are shorter than the other ring C–C bond lengths {all greater than 1.40 Å} and in the range expected for a semiquinone.¹⁷

By contrast, the C–O bond distances of the *o*-O₂C₆Cl₄ ligand of the (majority) *N*-bound Ru(CO)₂(PPh₃)(*o*-O₂C₆Cl₄) fragment {C(19)–O(1) = 1.334(7) and C(24)–O(2) = 1.311(7) Å} are similar to the values found for catecholate complexes such as [NEt₄]⁺**1**[–], [NEt₄]⁺**8**[–], [(*o*-O₂C₆Cl₄)(Ph₃P)(OC)₂Ru(μ-NC)Mn(CO)₂(PEt₃)(dppe)-*cis*]⁶ and [(*o*-O₂C₆Cl₄)(Ph₃P)(OC)₂Ru(μ-NC)Re(CO)₃(*o*-phen)]⁷. Thus, one can deduce that [NEt₄]⁺**8**[–] is first oxidised at the *C*-bound ruthenium fragment (assuming that the disposition of the catecholate and semiquinone fragments reflects the predominant component of the disordered cyanide bridge).

Unlike in the structure of **8**[–], the bend in the cyanide bridge serves to move the two mutually *cis* O₂C₆Cl₄ ligands towards each other; the distance between the C₆ ring centroids is 3.74 Å, and the angle between their mean planes is 12.6°. There also appears to be a π-interaction between each O₂C₆Cl₄ ligand and a phenyl ring from an adjacent triphenylphosphine ligand (centroid–centroid ring distances 3.44 and 3.69 Å, with the angles between the rings 11.8 and 23.1°). Moreover, the interaction seems to be stronger between the semiquinone form of the O₂C₆Cl₄ ligand and its adjacent phenyl ring; *i.e.* the centroid–centroid ring distance is 3.44 Å and the two rings are more parallel.

The structure of **9A** is similar to that of **8** in that each ruthenium atom is bound, in a slightly distorted octahedral environment, to two carbonyl ligands, two oxygen atoms of the *o*-O₂C₆Cl₄ ligand, the phosphorus atom of PPh₃ or P(OPh)₃, and the cyanide bridge. As in **8**, the bond lengths in the two *o*-O₂C₆Cl₄ ligands are different; the C–O bond distances of the *o*-O₂C₆Cl₄ ligand at the *C*-bound end of the cyanide bridge {C(19)–O(1) = 1.312(12), C(24)–O(2) = 1.296(12) Å} and at the *N*-bound end {C(28)–O(5) = 1.356(13), C(33)–O(6) = 1.323(13) Å} are consistent with a semiquinone and a catecholate respectively (*i.e.* the oxidised *o*-O₂C₆Cl₄ ligand is at the *C*-bound ruthenium fragment). However, the structure of **9A** is highly unusual in that the P(OPh)₃ ligand at the *N*-bound Ru(CO)₂{P(OPh)₃}(*o*-O₂C₆Cl₄) fragment is *cis* to the cyanide bridge, and therefore different from all other related complexes in which the *P*-donor ligand is *trans* to the cyanide, *i.e.* as in [NEt₄][Ru(CN)(CO)₂(PPh₃)(*o*-O₂C₆Cl₄)] [NEt₄]⁺**1**[–], [(*o*-O₂C₆Cl₄)(Ph₃P)(OC)₂Ru(μ-NC)Mn(CO)₂(PEt₃)(dppe)-*cis*]⁶, [(*o*-O₂C₆Cl₄)(Ph₃P)(OC)₂Ru(μ-NC)Re(CO)₃(*o*-phen)]⁷, [NEt₄]⁺**8**[–] and **8**.

Interestingly, the same type of inter-ring interaction is observed as described for **8** above. Thus, although there is no such stacking possible between the catecholate ring and a phenyl group of the P(OPh)₃ ligand (because of the isomerisation noted above), the semiquinone ligand and one phenyl ring of the PPh₃ ligand are canted towards each other; the centroid–centroid ring distance, *d*, is 3.34 Å, and the angle, *a*, between the two rings is 5.6°. Such interactions are also observed in [Ru(CO)₂(PPh₃)₂(*o*-O₂C₆Cl₄)]⁺, where the axial P–Ru–P core is slightly bent so that one phenyl ring of each of the two phosphines interacts with the semiquinone (the P–Ru–P axis is bent in the opposite sense in the neutral catecholate complex [Ru(CO)₂(PPh₃)₂(*o*-O₂C₆Cl₄)]⁰ and in [Rh(*o*-O₂C₆Cl₄)(PPh₃)Tp]⁺{Tp[–] = hydrotris(3,5-dimethylpyrazolyl)borate; *d* = 3.26 Å, *a* = 7.8°}; the neutral complex [Rh(*o*-O₂C₆Cl₄)(PPh₃)Tp] shows no such interaction.¹⁸ Moreover, similar interactions in the crystal structure of [Cr(*o*-O₂C₆Cl₄)₃].0.5C₆H₆.CS₂ result in almost perfect stacking of the benzene ring between two semiquinone rings of two different [Cr(*o*-O₂C₆Cl₄)₃] molecules (*d* = 3.50 Å, *a* = 5.0°).¹⁹

Isomerisation involving movement of the P(OPh)₃ ligand from a position *cis* to both oxygen atoms of *o*-O₂C₆Cl₄ (as in **9**[–]) to *trans* to one of them could occur at any one of several steps in the formation of **9A**. In the dimer [{Ru(CO)₂{P(OPh)₃}(μ-*o*-O₂C₆Cl₄)]₂, the *cis*-(CO)₂ ligands are *trans* to the oxygen atoms of the catecholate ligand so bridge-cleavage with [NEt₄]⁺**1**[–] should give the product with *N*-bound cyanide *trans* to P(OPh)₃. The ³¹P NMR spectrum of [NEt₄]⁺**9**[–] (see above) shows that only one isomer is formed and as the chemical shift for the phosphorus atom of the PPh₃ ligand is the same for **8**[–] and **9**[–], as is *J*_{PP}, it seems likely that the same isomer, *i.e.* with a *trans*-P–Ru–CN–Ru–P skeleton, is formed. {One might expect the chemical shift of PPh₃, and *J*_{PP}, to differ in the skeleton *trans*-(OC)–Ru–CN–Ru–PPh₃ found in **9A**.} Thus, isomerisation during the bridge-cleavage reaction with [{Ru(CO)₂{P(OPh)₃}(μ-*o*-O₂C₆Cl₄)]₂ to form **9**[–] seems unlikely.

It is noteworthy that an IR spectro-electrochemical study of the stepwise one-electron oxidation of **9**[–] to **9** and then subsequent stepwise reduction, showed **9** and **9**[–] to be reversibly regenerated, *i.e.* isomerisation does not occur on the timescale of electrolysis (*ca.* 30 min). It therefore seems most likely that isomerisation of **9** (with the same structure as **8**) to **9A**, the structurally

characterised complex, occurred over the three weeks required for crystallisation.

Conclusions

The complexes $[\text{NEt}_4][(\text{o-O}_2\text{C}_6\text{Cl}_4)\text{L}(\text{OC})_2\text{Ru}(\mu\text{-CN})\text{Ru}(\text{CO})_2\text{-L}'(\text{o-O}_2\text{C}_6\text{Cl}_4)]$ {L or L' = PPh₃ or P(OPh)₃} undergo two sequential one-electron oxidations at the catecholate ligands to give the isolable neutral $[(\text{o-O}_2\text{C}_6\text{Cl}_4)\text{L}(\text{OC})_2\text{Ru}(\mu\text{-CN})\text{Ru}(\text{CO})_2\text{L}'(\text{o-O}_2\text{C}_6\text{Cl}_4)]$ and cationic $[(\text{o-O}_2\text{C}_6\text{Cl}_4)\text{L}(\text{OC})_2\text{Ru}(\mu\text{-CN})\text{Ru}(\text{CO})_2\text{-L}'(\text{o-O}_2\text{C}_6\text{Cl}_4)]^+$ complexes, containing one and two semiquinone ligands respectively. The order of oxidation of the two centres depends on L, L' and the orientation of the cyanide bridge with the linkage isomers $[(\text{o-O}_2\text{C}_6\text{Cl}_4)(\text{Ph}_3\text{P})(\text{OC})_2\text{Ru}(\mu\text{-CN})\text{-Ru}(\text{CO})_2\{\text{P}(\text{OPh})_3\}(\text{o-O}_2\text{C}_6\text{Cl}_4)]^-$ and $[(\text{o-O}_2\text{C}_6\text{Cl}_4)\{\text{(PhO)}_3\text{P}\}(\text{OC})_2\text{Ru}(\mu\text{-CN})\text{Ru}(\text{CO})_2\{\text{PPh}_3\}(\text{o-O}_2\text{C}_6\text{Cl}_4)]^-$ oxidised at the C- and N-bonded $\text{Ru}(\text{CO})_2\{\text{PPh}_3\}(\text{o-O}_2\text{C}_6\text{Cl}_4)$ units respectively. Structural studies on $[(\text{o-O}_2\text{C}_6\text{Cl}_4)(\text{Ph}_3\text{P})(\text{OC})_2\text{Ru}(\mu\text{-CN})\text{-Ru}(\text{CO})_2\{\text{PPh}_3\}(\text{o-O}_2\text{C}_6\text{Cl}_4)]$ confirm oxidation at the C-bound $\text{Ru}(\text{CO})_2(\text{o-O}_2\text{C}_6\text{Cl}_4)$ fragment whereas the ESR spectrum of $[(\text{o-O}_2\text{C}_6\text{Cl}_4)\{\text{(PhO)}_3\text{P}\}(\text{OC})_2\text{Ru}(\mu\text{-CN})\text{Ru}(\text{CO})_2\{\text{PPh}_3\}(\text{o-O}_2\text{C}_6\text{Cl}_4)]$ is consistent with an N-bound $\text{Ru}(\text{CO})_2(\text{o-O}_2\text{C}_6\text{Cl}_4)$ semiquinone fragment. A structural study of $[(\text{o-O}_2\text{C}_6\text{Cl}_4)(\text{Ph}_3\text{P})(\text{OC})_2\text{Ru}(\mu\text{-CN})\text{Ru}(\text{CO})_2\{\text{P}(\text{OPh})_3\}(\text{o-O}_2\text{C}_6\text{Cl}_4)]$, while showing oxidation of C-bound $\text{Ru}(\text{CO})_2(\text{o-O}_2\text{C}_6\text{Cl}_4)$, also revealed unprecedented migration of P(OPh)₃ to a position *cis* to the cyanide bridge (contrasting with the normal *trans* P-donor arrangement in $[(\text{o-O}_2\text{C}_6\text{Cl}_4)(\text{Ph}_3\text{P})(\text{OC})_2\text{Ru}(\mu\text{-CN})\text{Ru}(\text{CO})_2\{\text{PPh}_3\}(\text{o-O}_2\text{C}_6\text{Cl}_4)]$).

Experimental

The preparation, purification and reactions of the complexes described were carried out under an atmosphere of dry nitrogen using deoxygenated solvents purified by using Anhydrous Engineering double alumina or alumina-copper catalyst drying columns. Reactions were monitored by IR spectroscopy. Unless stated otherwise, complexes were (i) purified by dissolving the impure solid in CH₂Cl₂, filtering the resulting solution, treating the filtrate with *n*-hexane, and reducing the volume of the mixture *in vacuo* to induce precipitation, and (ii) are air-stable solids which dissolve in polar solvents such as CH₂Cl₂ or thf to give moderately air-stable solutions.

The compounds, $[\{\text{Ru}(\text{CO})_2(\text{PPh}_3)(\mu\text{-o-O}_2\text{C}_6\text{Cl}_4)\}_2]^+$ and $[\text{Fe}(\eta\text{-C}_5\text{H}_4\text{COME})(\eta\text{-C}_5\text{H}_5)][\text{BF}_4]^{20}$ were prepared by published methods. The compounds $[\text{NEt}_4]\text{CN}$ and tetrachlorobenzene-*o*-quinone (*o*-chloranil) were purchased from Aldrich and Lancaster Chemicals respectively.

IR spectra were recorded on a Perkin Elmer Spectrum One FT spectrometer fitted with a Perkin Elmer ZnSe universal ATR sampling accessory; NMR spectra were recorded on a JEOL λ 300 spectrometer. X-Band ESR spectra were recorded on a Bruker ESP300E spectrometer equipped with a Hewlett-Packard 5350B microwave frequency counter. The field calibration was checked by measuring the resonance of the diphenylpicrylhydrazyl (dpph) radical before each series of spectra. Spectra were simulated using the Bruker Simfonia programme.

Cyclic voltammetry was carried out using an EG & G Model 273A potentiostat linked to a computer using EG & G Model 270 Research Electrochemistry software in conjunction with a three-

electrode cell. The auxiliary electrode was a platinum wire and the working electrode a platinum disc (1.6 mm diameter). The reference electrode was an aqueous saturated calomel electrode separated from the test solution by a fine porosity frit and an agar bridge saturated with KCl. Solutions, in CH₂Cl₂, were 1.0×10^{-3} mol dm⁻³ in the compound and 0.1 mol dm⁻³ in $[\text{NBu}_4][\text{PF}_6]$ as the supporting electrolyte. Under these conditions, E_o' for the one-electron oxidation of $[\text{Fe}(\eta\text{-C}_5\text{H}_4\text{COME})(\eta\text{-C}_5\text{H}_5)]$, $[\text{Fe}(\eta\text{-C}_5\text{H}_5)_2]$ or $[\text{Fe}(\eta\text{-C}_5\text{Me}_5)_2]$, added to the test solutions as internal calibrants, is 0.74, 0.47 and -0.08 V respectively.

Microanalyses were carried out by the staff of the Microanalytical Service of the School of Chemistry, University of Bristol.

Syntheses

$[\text{Ru}(\text{CO})_2\{\text{P}(\text{OPh})_3\}(\eta\text{-C}_4\text{H}_4\text{Me}_2)]$. A mixture of $[\text{Ru}_3(\text{CO})_{12}]$ (2.0 g, 3.13 mmol) and 2,3-dimethylbuta-1,3-diene (5 cm³, 9.5 mmol) in *n*-heptane (100 cm³) was heated under reflux for 23 h. The colourless solution was cooled to room temperature, P(OPh)₃ (3.7 cm³, 7.63 mmol) was added and then the mixture was heated under reflux for 6 d. The yellow solution was evaporated to dryness *in vacuo* and the yellow residue dissolved in the minimum volume of CH₂Cl₂ (*ca.* 5 cm³) and placed on an alumina-*n*-hexane chromatography column. Elution with *n*-hexane gave a small amount of $[\text{Ru}(\text{CO})_3(\eta\text{-C}_4\text{H}_4\text{Me}_2)]$; elution with *n*-hexane-diethyl ether (20 : 1) gave a colourless solution of $[\text{Ru}(\text{CO})_2\{\text{P}(\text{OPh})_3\}(\eta\text{-C}_4\text{H}_4\text{Me}_2)]$ which was evaporated to dryness *in vacuo*. Purification gave the product as a white solid, yield 1.63 g (32%). ¹H NMR (CD₂Cl₂): δ 7.0–7.3 {m, 15H, P(OPh)₃}, 2.58 (m, 4H, C₄H₄Me₂), 1.54 (s, 6H, C₄H₄Me₂).

$[\{\text{Ru}(\text{CO})_2\{\text{P}(\text{OPh})_3\}(\mu\text{-o-O}_2\text{C}_6\text{Cl}_4)\}_2]$. To a stirred solution of $[\text{Ru}(\text{CO})_2\{\text{P}(\text{OPh})_3\}(\eta\text{-C}_4\text{H}_4\text{Me}_2)]$ (835 mg, 1.52 mmol) in CH₂Cl₂ (40 cm³) was added *o*-chloranil (374 mg, 1.52 mmol). After 15 min, the orange solution was filtered, *n*-hexane (50 cm³) was added and the volume of the solvent was reduced *in vacuo* to complete precipitation. Purification gave the product as an orange solid, yield 880 mg (79%).

$[\text{NEt}_4][\text{Ru}(\text{CN})(\text{CO})_2(\text{PPh}_3)(\text{o-O}_2\text{C}_6\text{Cl}_4)]$ $[\text{NEt}_4]^+1^-$. To a stirred solution of $[\{\text{Ru}(\text{CO})_2(\text{PPh}_3)(\mu\text{-o-O}_2\text{C}_6\text{Cl}_4)\}_2]$ (200 mg, 0.15 mmol) in CH₂Cl₂ (30 cm³) was added $[\text{NEt}_4]\text{CN}$ (47 mg, 0.30 mmol). After 10 min, the yellow solution was filtered, *n*-hexane (40 cm³) was added, and the volume of the solvent was reduced *in vacuo* to complete precipitation. Purification gave the product as a yellow solid, yield 104 mg (68%).

The complex $[\text{NEt}_4][\text{Ru}(\text{CN})(\text{CO})_2\{\text{P}(\text{OPh})_3\}(\text{o-O}_2\text{C}_6\text{Cl}_4)]$ $[\text{NEt}_4]^+2^-$ was prepared similarly.

$[\text{Ru}(\text{CO})_2(\text{NCMe})(\text{PPh}_3)(\text{o-O}_2\text{C}_6\text{Cl}_4)]$. The dimer $[\{\text{Ru}(\text{CO})_2(\text{PPh}_3)(\mu\text{-o-O}_2\text{C}_6\text{Cl}_4)\}_2]$ (35 mg, 0.02 mmol) was dissolved in MeCN (20 cm³). After 10 min, the yellow solution was filtered and the filtrate evaporated to dryness *in vacuo*. The yellow residue was dissolved in CH₂Cl₂ (10 cm³), *n*-hexane (30 cm³) was added and the volume of the solvent was reduced *in vacuo* to complete precipitation. Purification gave the product as a yellow solid, yield 20 mg (54%).

$[\text{Ru}(\text{CO})_2\{\text{P}(\text{OPh})_3\}_2(\text{o-O}_2\text{C}_6\text{Cl}_4)]$. To a stirred solution of $[\{\text{Ru}(\text{CO})_2\{\text{P}(\text{OPh})_3\}(\mu\text{-o-O}_2\text{C}_6\text{Cl}_4)\}_2]$ (45 mg, 0.03 mmol) in CH₂Cl₂ (20 cm³) was added P(OPh)₃ (0.12 cm³, 0.06 mmol). After

10 min, the yellow solution was filtered, *n*-hexane (30 cm³) was added and the volume of the solvent was reduced *in vacuo* to complete precipitation. Purification gave the product as a yellow solid, yield 30 mg (46%).

[NEt₄][(o-O₂C₆Cl₄)(Ph₃P)(OC)₂Ru(μ-CN)Ru(CO)₂(PPh₃)(o-O₂C₆Cl₄)] [NEt₄]⁺8⁻. To a stirred solution of [{Ru(CO)₂(PPh₃)(μ-o-O₂C₆Cl₄)₂] (102 mg, 0.07 mmol) in CH₂Cl₂ (20 cm³) was added [NEt₄][Ru(CN)(CO)₂(PPh₃)(o-O₂C₆Cl₄)] (126 mg, 0.16 mmol). After 10 min, the yellow solution was filtered, *n*-hexane (20 cm³) was added and the volume of solvent reduced *in vacuo* to complete precipitation. Purification gave the product as a yellow solid, yield 157 mg (66%).

The complexes [NEt₄][(o-O₂C₆Cl₄)(Ph₃P)(OC)₂Ru(μ-CN)Ru(CO)₂{P(OPh)₃}(o-O₂C₆Cl₄)] [NEt₄]⁺9⁻, [NEt₄][(o-O₂C₆Cl₄)(PhO)₃P}(OC)₂Ru(μ-CN)Ru(CO)₂{P(OPh)₃}(o-O₂C₆Cl₄)] [NEt₄]⁺10⁻ and [NEt₄][(o-O₂C₆Cl₄)(PhO)₃P}(OC)₂Ru(μ-CN)Ru(CO)₂(PPh₃)(o-O₂C₆Cl₄)] [NEt₄]⁺11⁻ were prepared similarly.

[(o-O₂C₆Cl₄)(Ph₃P)(OC)₂Ru(μ-CN)Ru(CO)₂(PPh₃)(o-O₂C₆Cl₄)] 8. To a stirred solution of [NEt₄][(o-O₂C₆Cl₄)(Ph₃P)(OC)₂Ru(μ-CN)Ru(CO)₂(PPh₃)(o-O₂C₆Cl₄)] (52 mg, 0.03 mmol) in CH₂Cl₂ (20 cm³) was added [Fe(η-C₅H₄COMe)(η-C₅H₅)] [BF₄] (11 mg, 0.03 mmol). After 15 min, the red solution was filtered and then evaporated to dryness. The residue was washed with *n*-hexane (2 × 10 cm³) and then purified to give a red solid, yield 20 mg (51%).

The complex [(o-O₂C₆Cl₄)(PhO)₃P}(OC)₂Ru(μ-CN)Ru(CO)₂{P(OPh)₃}(o-O₂C₆Cl₄)] **10** was prepared similarly.

[(o-O₂C₆Cl₄)(Ph₃P)(OC)₂Ru(μ-CN)Ru(CO)₂(PPh₃)(o-O₂C₆Cl₄)] [BF₄]⁺8⁻[BF₄]⁻. To a stirred solution of [NEt₄][(o-O₂C₆Cl₄)(Ph₃P)(OC)₂Ru(μ-CN)Ru(CO)₂(PPh₃)(o-O₂C₆Cl₄)] (50 mg, 0.03 mmol) in CH₂Cl₂ (20 cm³) was added [Fe(η-C₅H₄COMe)(η-C₅H₅)] [BF₄] (25 mg, 0.07 mmol). After 15 min, the red solution was filtered and then evaporated to dryness. The residue was

washed with *n*-hexane (2 × 10 cm³) and then purified to give a purple solid, yield 30 mg (68%).

The complexes [(o-O₂C₆Cl₄)(Ph₃P)(OC)₂Ru(μ-CN)Ru(CO)₂{P(OPh)₃}(o-O₂C₆Cl₄)] [BF₄]⁺9⁻[BF₄]⁻, [(o-O₂C₆Cl₄)(PhO)₃P}(OC)₂Ru(μ-CN)Ru(CO)₂{P(OPh)₃}(o-O₂C₆Cl₄)] [BF₄]⁺10⁻[BF₄]⁻ and [(o-O₂C₆Cl₄)(PhO)₃P}(OC)₂Ru(μ-CN)Ru(CO)₂(PPh₃)(o-O₂C₆Cl₄)] [BF₄]⁺11⁻[BF₄]⁻ were prepared similarly.

[(o-O₂C₆Cl₄)(Ph₃P)(OC)₂Ru(μ-CN)Ru(CO)₂{P(OPh)₃}(o-O₂C₆Cl₄)] 9. To a stirred solution of [NEt₄][(o-O₂C₆Cl₄)(Ph₃P)(OC)₂Ru(μ-CN)Ru(CO)₂{P(OPh)₃}(o-O₂C₆Cl₄)] (34 mg, 0.02 mmol) in CH₂Cl₂ (20 cm³) was added [(o-O₂C₆Cl₄)(Ph₃P)(OC)₂Ru(μ-CN)Ru(CO)₂{P(OPh)₃}(o-O₂C₆Cl₄)] [BF₄]⁺ (33 mg, 0.02 mmol). After 15 min, the red solution was evaporated to dryness and then the residue was extracted with diethyl ether (15 cm³). The extract was filtered through Celite and then the volume of the filtrate was reduced to ca. 3 cm³ before *n*-hexane was added to precipitate the product as a red solid, yield 44 mg (72%).

The complex [(o-O₂C₆Cl₄)(PhO)₃P}(OC)₂Ru(μ-CN)Ru(CO)₂(PPh₃)(o-O₂C₆Cl₄)] **11** was prepared similarly.

Crystal structure determinations of [Ru(CO)₂{P(OPh)₃}(μ-o-O₂C₆Cl₄)₂], [NEt₄][Ru(CN)(CO)(PPh₃)(o-O₂C₆Cl₄)]·0.5CH₂Cl₂, [NEt₄]⁺1⁻·0.5CH₂Cl₂, [NEt₄][(o-O₂C₆Cl₄)(Ph₃P)(OC)₂Ru(μ-CN)Ru(CO)₂(PPh₃)(o-O₂C₆Cl₄)]·0.5CH₂Cl₂, [NEt₄]⁺8⁻·0.5CH₂Cl₂, [(o-O₂C₆Cl₄)(Ph₃P)(OC)₂Ru(μ-CN)Ru(CO)₂(PPh₃)(o-O₂C₆Cl₄)]·CH₂Cl₂, **8·CH₂Cl₂ and [(o-O₂C₆Cl₄)(Ph₃P)(OC)₂Ru(μ-CN)Ru(CO)₂{P(OPh)₃}(o-O₂C₆Cl₄)]·2CH₂Cl₂, **9A**·2CH₂Cl₂**

Yellow crystals of [Ru(CO)₂{P(OPh)₃}(μ-o-O₂C₆Cl₄)₂] and of [NEt₄][Ru(CN)(CO)(PPh₃)(o-O₂C₆Cl₄)]·0.5CH₂Cl₂ [NEt₄]⁺1⁻·0.5CH₂Cl₂ were grown by allowing *n*-hexane to diffuse into a concentrated CH₂Cl₂ solution of the complex at -10 °C. Yellow crystals of [NEt₄][(o-O₂C₆Cl₄)(Ph₃P)(OC)₂Ru(μ-CN)Ru(CO)₂(PPh₃)(o-O₂C₆Cl₄)]·0.5CH₂Cl₂ [NEt₄]⁺8⁻·0.5CH₂Cl₂ were grown

Table 10 Crystal and refinement data for [Ru(CO)₂{P(OPh)₃}(μ-o-O₂C₆Cl₄)₂], [NEt₄][Ru(CN)(CO)(PPh₃)(o-O₂C₆Cl₄)]·0.5CH₂Cl₂, [NEt₄]⁺1⁻·0.5CH₂Cl₂, [NEt₄][(o-O₂C₆Cl₄)(Ph₃P)(OC)₂Ru(μ-CN)Ru(CO)₂(PPh₃)(o-O₂C₆Cl₄)]·0.5CH₂Cl₂, [NEt₄]⁺8⁻·0.5CH₂Cl₂, [(o-O₂C₆Cl₄)(Ph₃P)(OC)₂Ru(μ-CN)Ru(CO)₂(PPh₃)(o-O₂C₆Cl₄)]·CH₂Cl₂, **8**·CH₂Cl₂ and [(o-O₂C₆Cl₄)(Ph₃P)(OC)₂Ru(μ-CN)Ru(CO)₂{P(OPh)₃}(o-O₂C₆Cl₄)]·2CH₂Cl₂, **9A**·2CH₂Cl₂

Compound	[Ru(CO) ₂ {P(OPh) ₃ }(μ-o-O ₂ C ₆ Cl ₄) ₂]	[NEt ₄] ⁺ 1 ⁻ ·0.5CH ₂ Cl ₂	[NEt ₄] ⁺ 8 ⁻ ·0.5CH ₂ Cl ₂	8 ·CH ₂ Cl ₂	9A ·2CH ₂ Cl ₂
Formula	C ₅₂ H ₃₀ Cl ₈ O ₁₄ P ₂ Ru ₂	C _{35.5} H ₃₆ N ₂ O ₄ RuPCl ₅	C _{69.5} H ₆₆ Cl ₉ N ₂ O ₈ P ₂ Ru ₂	C ₅₄ H ₃₂ Cl ₁₀ NO ₈ P ₂ Ru ₂	C ₅₃ H ₃₄ Cl ₁₂ NO ₁₁ P ₂ Ru ₂
<i>M</i>	1426.44	863.95	1640.37	1441.39	1574.31
Crystal system	Triclinic	Triclinic	Monoclinic	Monoclinic	Triclinic
Space group (no.)	<i>P</i> $\bar{1}$ (2)	<i>P</i> $\bar{1}$ (2)	<i>C</i> (2)/ <i>c</i> (15)	<i>P</i> 2(1)/ <i>c</i> (14)	<i>P</i> $\bar{1}$ (2)
<i>a</i> /Å	10.627(2)	13.9435(6)	62.9641(11)	14.9280(9)	12.433(12)
<i>b</i> /Å	13.614(3)	15.6637(7)	9.5138(2)	25.8112(16)	14.524(12)
<i>c</i> /Å	19.419(4)	18.5668(8)	24.0104(4)	16.5709(10)	17.893(16)
<i>a</i> /°	92.28(3)	95.542(1)	90	90	82.55(3)
<i>β</i> /°	90.11(3)	110.313(1)	93.624(1)	110.103(1)	72.74(3)
<i>γ</i> /°	106.27(3)	94.399(1)	90	90	77.12(3)
<i>T</i> /K	173(2)	173(2)	173(2)	173(2)	100(2)
<i>U</i> /Å ³	2694.6(9)	3758.7(3)	14354.1(5)	5995.9(6)	3001(5)
<i>Z</i>	2	4	8	4	2
<i>λ</i> /Å	0.71073	0.71073	1.54178	0.71073	1.54178
<i>μ</i> /mm ⁻¹	1.083	0.856	7.356	1.054	10.005
Reflections collected	31250	40476	53177	39116	22595
Independent reflections (<i>R</i> _{int})	12331 (0.0210)	17132 (0.0557)	13265 (0.0691)	13750 (0.1170)	9530 (0.0975)
Final <i>R</i> indices [<i>I</i> > 2σ(<i>I</i>)]:	0.0270, 0.0605	0.0438, 0.0820	0.0339, 0.0783	0.0622, 0.1161	0.0687, 0.1800
<i>R</i> ₁ , <i>wR</i> ₂					

by allowing diethyl ether to diffuse into a concentrated CH_2Cl_2 solution at -10°C . Red crystals of $[(o\text{-O}_2\text{C}_6\text{Cl}_4)(\text{Ph}_3\text{P})(\text{OC})_2\text{Ru}(\mu\text{-CN})\text{Ru}(\text{CO})_2(\text{PPh}_3)(o\text{-O}_2\text{C}_6\text{Cl}_4)]\cdot\text{CH}_2\text{Cl}_2$ **8** $\cdot\text{CH}_2\text{Cl}_2$ and $[(o\text{-O}_2\text{C}_6\text{Cl}_4)(\text{Ph}_3\text{P})(\text{OC})_2\text{Ru}(\mu\text{-CN})\text{Ru}(\text{CO})_2\{\text{P}(\text{O}^i\text{Pr})_3\}(o\text{-O}_2\text{C}_6\text{Cl}_4)]\cdot 2\text{CH}_2\text{Cl}_2$ **9A** $\cdot 2\text{CH}_2\text{Cl}_2$ were grown by allowing diethyl ether to diffuse into a concentrated CH_2Cl_2 solution, of **8** and **9** respectively, at -10°C .

Many of the details of the structure analyses of $[\{\text{Ru}(\text{CO})_2\text{-}\{\text{P}(\text{O}^i\text{Pr})_3\}(\mu\text{-}o\text{-O}_2\text{C}_6\text{Cl}_4)\}_2]$, $[\text{NEt}_4]^+\text{I}^- \cdot 0.5\text{CH}_2\text{Cl}_2$, $[\text{NEt}_4]^+\text{8}^- \cdot 0.5\text{CH}_2\text{Cl}_2$, **8** $\cdot\text{CH}_2\text{Cl}_2$ and **9A** $\cdot 2\text{CH}_2\text{Cl}_2$ are listed in Table 10. The orientation of the cyanide bridges in complexes **8** and **8** $^-$ was assigned on the basis of the best agreement for the thermal parameters and occupancy factors for the C and N atoms, after refinement in two alternative models in which the C and N atoms were exchanged. This led to a 50 : 50 ratio of CN to NC in **8** $^-$, and a 65(7) : 35(7) ratio in **8**. The structure of $[\text{NEt}_4]^+\text{I}^- \cdot 0.5\text{CH}_2\text{Cl}_2$ contains two I^- anions, two $[\text{NEt}_4]^+$ cations (one of which is disordered over two positions) and one disordered molecule of CH_2Cl_2 in the asymmetric unit. The CH_2Cl_2 molecule in the structure of $[\text{NEt}_4]^+\text{8}^- \cdot 0.5\text{CH}_2\text{Cl}_2$ is also disordered over two positions.

CCDC reference numbers 633571–633575.

For crystallographic data in CIF or other electronic format see DOI: 10.1039/b700648a

Acknowledgements

We thank UUK for an ORS Postgraduate Scholarship (to S.O.), the Royal Thai Government for a Postgraduate Scholarship (to A.K.) and Dr S. Vickers and Prof. M.D. Ward of the University of Sheffield for the IR spectroelectrochemical study of the oxidation of $[\text{NEt}_4][\{(o\text{-O}_2\text{C}_6\text{Cl}_4)(\text{Ph}_3\text{P})(\text{OC})_2\text{Ru}(\mu\text{-CN})\text{Ru}(\text{CO})_2\text{-}\{\text{P}(\text{O}^i\text{Pr})_3\}(o\text{-O}_2\text{C}_6\text{Cl}_4)\}] [\text{NEt}_4]^+\text{9}^-$.

References

1 See, for example, G. A. Carriedo, N. G. Connelly, M. C. Crespo, I. C. Quarmby, V. Riera and G. H. Worth, *J. Chem. Soc., Dalton Trans.*, 1991,

- 315; G. A. Carriedo, N. G. Connelly, S. Alvarez, E. Perez-Carreno and S. Garcia-Granda, *Inorg. Chem.*, 1993, **32**, 272; F. L. Atkinson, A. Christofides, N. G. Connelly, H. J. Lawson, A. C. Loyns, A. G. Orpen, G. M. Rosair and G. H. Worth, *J. Chem. Soc., Dalton Trans.*, 1993, 1441; F. L. Atkinson, N. C. Brown, N. G. Connelly, A. G. Orpen, A. L. Rieger, P. H. Rieger and G. M. Rosair, *J. Chem. Soc., Dalton Trans.*, 1996, 1959; M. Bardaji, N. C. Brown, A. Christofides and N. G. Connelly, *J. Chem. Soc., Dalton Trans.*, 1996, 2511; N. C. Brown, G. B. Carpenter, N. G. Connelly, J. G. Crossley, A. Martin, A. G. Orpen, A. L. Rieger, P. H. Rieger and G. H. Worth, *J. Chem. Soc., Dalton Trans.*, 1996, 3977; K. M. Anderson, N. G. Connelly, E. Llamas-Rey, A. G. Orpen and R. L. Paul, *Chem. Commun.*, 2001, 1734; C. J. Adams, K. M. Anderson, M. Bardaji, N. G. Connelly, N. J. Goodwin, E. Llamas-Rey, A. G. Orpen and P. H. Rieger, *Dalton Trans.*, 2004, 683.
- 2 C. J. Adams, N. G. Connelly, N. J. Goodwin, O. D. Hayward, A. G. Orpen and A. J. Wood, *Dalton Trans.*, 2006, 3584.
- 3 N. G. Connelly, I. Manners, J. R. C. Protheroe and M. W. Whiteley, *J. Chem. Soc., Dalton Trans.*, 1984, 2713.
- 4 R. M. Buchanan and C. G. Pierpont, *Inorg. Chem.*, 1979, **18**, 1616.
- 5 S. C. Shoner and P. P. Power, *Inorg. Chem.*, 1992, **31**, 1001.
- 6 A. Christofides, N. G. Connelly, H. J. Lawson, A. C. Loyns, A. G. Orpen, M. O. Simmonds and G. H. Worth, *J. Chem. Soc., Dalton Trans.*, 1991, 1595.
- 7 M. Bardaji, N. C. Brown, N. G. Connelly, R. Davies, A. G. Orpen, G. M. Rosair and N. R. Seear, *J. Organomet. Chem.*, 1994, **474**, C21.
- 8 C. G. Pierpont and H. H. Downs, *Inorg. Chem.*, 1975, **14**, 343.
- 9 M. J. Freeman, PhD Thesis, University of Bristol, 1984.
- 10 A. P. Meacham, K. L. Druce, Z. R. Bell, M. D. Ward, J. B. Keister and A. B. P. Lever, *Inorg. Chem.*, 2003, **42**, 7887.
- 11 G. A. Carriedo, M. C. Crespo, V. Riera, M. G. Sanchez, M. L. Valin, D. Moreiras and X. Solans, *J. Organomet. Chem.*, 1986, **302**, 47.
- 12 L. Pasimeni, M. Brustolon and C. Corvaja, *J. Magn. Reson.*, 1976, **21**, 259.
- 13 D. A. Dows, A. Haim and W. K. Waltham, *J. Inorg. Nucl. Chem.*, 1961, **21**, 33.
- 14 S. Bhattacharya and C. G. Pierpont, *Inorg. Chem.*, 1994, **33**, 6038.
- 15 S. Bhattacharya and C. G. Pierpont, *Inorg. Chem.*, 1991, **30**, 1511.
- 16 T. Wada, T. Fujihara, M. Tomori, D. Ooyama and K. Tanaka, *Bull. Chem. Soc. Jpn.*, 2004, **77**, 741.
- 17 S. R. Boone, G. H. Purser, H.-R. Chang, M. D. Lowery, D. N. Hendrickson and C. G. Pierpont, *J. Am. Chem. Soc.*, 1989, **111**, 2292.
- 18 N. G. Connelly, D. J. H. Emslie, O. D. Hayward, A. G. Orpen and M. J. Quayle, *J. Chem. Soc., Dalton Trans.*, 2001, 875.
- 19 C. G. Pierpont and H. H. Downs, *J. Am. Chem. Soc.*, 1976, **98**, 4834.
- 20 N. G. Connelly and W. E. Geiger, *Chem. Rev.*, 1996, **96**, 877.